AIMS Mathematics, 11(7): 22688–22723.
DOI: 10.3934/math.2026916
Received: 11 April 2026
Revised: 02 July 2026
Accepted: 14 July 2026
Published: 28 July 2026

http://www.aimspress.com/journal/Math

*Research article*

# A data-driven mathematical modeling framework for predicting HIV/HBV coinfection dynamics using machine learning approaches

**Muhammad Asad Ullah[1], Sana Ullah Saqib[2,*], Yin-Tzer Shih[2,*], Nermeen Abdullah[3], Nidhal Becheikh[4], Lioua Kolsi[5] and Kaouther Ghachem[3]**

[1] Institute for Advanced Study in Nuclear Energy & Safety, College of Physics and Optoelectronic Engineering, Shenzhen University, Shenzhen, 518060, China

[2] Department of Applied Mathematics, National Chung Hsing University, Taichung 402202, Taiwan

[3] Department of Industrial and Systems Engineering, College of Engineering, Princess Nourah bint Abdulrahman University, P. O. Box 84428, Riyadh, 11671, Saudi Arabia

[4] Mining Research Center, Northern Border University, P. O. Box 1321, Arar 91431, Saudi Arabia

[5] Department of Mechanical Engineering, College of Engineering, University of Ha'il, Ha'il City 81451, Saudi Arabia

* **Correspondence:** Email: sanaullah0557@gmail.com, yintzer_shih@email.nchu.edu.tw; Tel: +886-4-2285-3459; Fax: +886-4-2287-3028.

**Abstract:** Viral coinfections remain a significant global health challenge, particularly when infections like human immunodeficiency virus (HIV) coexist with other diseases, causing coinfection in a single individual. This study develops a fractional-order multi-stage HIV/HBV coinfection model using the Caputo fractional derivative to capture memory effects in disease transmission and progression. The model includes latent, asymptomatic, and symptomatic infection stages, as well as key epidemiological factors, including the effects of HBV vaccination, recovery processes among asymptomatic and fully-infected HBV individuals, and the acquisition of secondary infections by exposed, asymptomatic, and individuals. The qualitative properties of the model, such as positivity, boundedness, and sensitivity of key parameters, are analyzed to evaluate the biological feasibility of the system. The basic reproduction numbers for HIV and HBV are calculated, and a sensitivity analysis is conducted to determine the primary parameters affecting coinfection transmission. The coinfected HIV/HBV model is numerically solved using an artificial neural network optimized by the Levenberg-Marquardt algorithm (ANN-LMA). The performance of the ANN-LMA scheme is evaluated using mean squared error (MSE), root mean square error (RMSE), regression analysis, training-state analysis, error histograms, and comparison of overlap results with reference numerical results, demonstrating minimal absolute error. The results underscore the significance of the proposed network in predicting complex coinfection

dynamics. This study provides policymakers and epidemic managers with a reliable modeling tool for developing adaptable and sustainable strategies to control HIV/HBV coinfection transmission.

**Keywords:** HIV/HBV coinfection model; comparison analysis; machine learning; simulation; fractional derivative; sensitivity analysis
**Mathematics Subject Classification:** 26A33, 34A08, 34A34, 65L20, 92D30

## 1. Introduction

Artificial intelligence (AI) strategies involve developing a computer-based decision support system that mimics human decision-making processes. Artificial neural networks (ANNs) are computational models inspired by biological processes that emulate the information processing mechanisms of the human brain. An ANN comprises multiple units, known as artificial neurons, which are interconnected by weights that collectively determine the network architecture. Although ANNs have advanced significantly, their creative capabilities remain markedly inferior to those of the human brain. The human brain is highly intricate, and, regrettably, numerous cognitive processes remain poorly understood. ANNs can handle vast amounts of data and produce predictions that are sometimes remarkably precise. ANNs offer a robust methodology for addressing complex computational challenges.

Artificial intelligence (AI) and machine learning (ML) have gained attention in epidemiology for analyzing large, complex datasets and uncovering hidden patterns in disease transmission [1]. Traditional epidemiological models typically depend on fixed assumptions and limited datasets. In contrast, ML techniques can analyze real-time data and enhance predictive accuracy for disease outbreaks. These techniques have been utilized to enhance public health decision-making, forecast epidemic trends, and estimate critical epidemiological parameters [2]. Moreover, AI-based models enhance the accuracy of disease spread predictions by integrating data from multiple sources, including medical records, migration patterns, demographic information, and climate data. Recent studies have increasingly applied machine learning and neural networks to enhance the performance of traditional mathematical models [3]. Guedri et al. [4] employed an ANN-based framework to describe ebola virus disease by adding disability compartment to the traditional SEIR model to account for long-term health problems. The ANN was trained on Runge–Kutta data using the Levenberg–Marquardt backpropagation algorithm to solve delay differential equations and generate accurate predictions of Ebola transmission. Chae et al. [5] forecasted infectious disease outbreaks by integrating social media and surveillance data through deep learning models, specifically deep neural networks (DNNs) and long short-term memory (LSTM) networks. The study demonstrated that deep learning methods surpass the traditional autoregressive integrated moving average (ARIMA) model in forecasting diseases such as chickenpox. The results indicate that AI-driven predictive models may improve responses to infectious disease outbreaks by reducing reporting delays in public health surveillance systems.

ANNs can be used effectively in simulating disease propagation in that they can capture complex and non-linear relations which might not be captured using conventional methods [6, 7]. The

use of networks such as DNN and LSTM models can be effectively utilized in predicting disease outbreaks and determining the factors leading to transmission by analyzing patterns in health-related and environmental data. ANNs can also learn from new patterns and can deal with diverse data ranging from case studies, demographic data, and even climate data [8]. ANNs have been applied to predict recent monkeypox outbreaks in several nations [9]. Besides this, physics-informed Neural Network (PINN)-based approaches have been utilized in predicting influenza epidemics and integrating mechanistic modeling into neural network training [10, 11]. Moreover, the PINN approach offers a combination of data-driven learning and knowledge of the processes underlying the process, leading to increased reliability of predictions [5, 12, 13]. PINNs have become a leading approach to epidemic modeling using neural networks. PINNs employ optimization techniques to epidemic dynamics models and address both forward and inverse problems within a unified framework. PINNs use optimization techniques to model epidemic dynamics and solve both forward and inverse problems within a single framework. PINNs offer a robust framework that combines data-driven learning with mechanical modeling, enabling accurate prediction and parameter estimation within a unified structure. PINNs offer a modern approach for solving complex epidemic modeling systems while simultaneously estimating unknown parameters. Unlike conventional numerical methods, PINNs can inherently handle incomplete data and parameter uncertainty. Increased reliability in predictions can be especially useful in creating interventions and optimizing resource allocation in case of outbreaks, which is critical to reduce the impact of such diseases on vulnerable groups. Asghar et al. [14] designed an ANN to study the dynamics of Neisseria meningitidis spread among the population consisting of five SVCIR compartments. The ANN was trained on data obtained via the Runge-Kutta method and tested via fitness tests, regression analysis, and error assessment. According to the findings, the ANN provided reliable, accurate predictions. Din et al. [15] introduced a stochastic HBV model including virus-to-cell and cell-to-cell transmissions. An ANN trained with the LMA was employed to simulate and analyze the spread of infection. Sabir et al. [16] designed the ANN-LMA model to examine complex patterns within a numerically simulated nonlinear influenza illness framework. The model yields highly accurate solutions that closely correspond to reference results across a range of conditions, including varying transmission rates and initial states in the influenza model.

Mathematical modeling is a key analytical tool in public health for managing infectious diseases. Infectious illnesses possess numerous transmission modalities. Certain infectious diseases are transmitted from one person to another. Certain diseases are conveyed by mosquitoes or other species of animals. Moreover, rotting food or contamination of water supplies may potentially lead to infectious disorders. The reliability of mathematical models for analyzing real-world phenomena is contingent upon the validity of their foundational assumptions and hypotheses. These situations present specific challenges that mathematical models can address. Epidemiological models are valuable tools for forecasting the spread of infectious diseases. They help identify key variables that affect illness management. Mathematical models have accurately predicted disease spread, though they have some limitations. The primary goal is to use an asymptotic framework to predict disease spread and enable timely preventive measures. Mathematical simulation of viral illnesses presents insights into the progression of a disease in later years. Numerous models have been developed to analyze the effects of viral infections on various populations. Mathematical models offer insights into the potential for an illness to grow into an epidemic and the methods that are offered to facilitate controlling it. The application of mathematical modeling is common in both technical and scientific sectors.

Mathematical modeling utilizing fractional calculus (FC) provides deeper insight into complex real-world phenomena [17, 18]. Recently, S.U. Saqib [19] developed a hybrid fractional order transmission model to analyze HIV dynamics among MSM in Taiwan. The model allows researchers to analyze illness transmission, assess its impact on populations, and evaluate the effectiveness of interventions to control the epidemic. Numerous biological and physical components in fractional-order systems exhibit significant sensitivity to initial conditions, resulting in chaotic behavior. The fractional derivative captures memory effects and provides a more accurate description of epidemic dynamics. Classical models often overlook key memory and hereditary factors in biological processes, such as incubation periods, waning immunity, and transmission history. The combination of fractional derivative systems with ANNs has been effective in modeling epidemics since it utilizes the memory effect together with data-driven learning methods. In doing so, complex nonlinear relations are discovered in big datasets [20]. The integration of FC with neural networks results in a mixed system that is adaptable like neural networks and which includes memory features due to the fact that fractional differential equations inherently involve memory properties. Such integration improves the accuracy and reliability of the prediction process, as well as helps to identify long-term patterns in disease transmission dynamics. Besides numerical analyses, deep neural networks (DNNs) help to validate and evaluate the model and also provide the number of people in different compartments, such as susceptible, infected, and recovered, over time in epidemic models [21, 22]. Such an integration improves the precision and reliability of predictions, as well as long-term trends in the transmission of diseases. In addition to conventional numeric calculations, DNNs enable the validation of the models and provide the possibility of calculating approximate solutions for compartments, for instance, the number of susceptibles, infectives, and recoveries in epidemics [23, 24]. Eiman et al. [25] studied a compartmental fractional-order model of rotavirus involving fractal fractional derivatives and deep neural networks. This approach led to precise predictions and validation of disease transmission dynamics. PINN architectures, which not only estimate epidemiological parameters, but also the order of fractional memory, perform better than traditional integer-order models regarding their explainability and prediction capability.

Nisar et al. [26] developed an ANN using a Caputo fractional-order model to analyze soil-transmitted helminth infection dynamics, focusing on sensitivity and stability assessment. Machine learning techniques enable accurate prediction of infection patterns and facilitate model validation. Caputo fractional derivatives provide a framework for analyzing the dynamics of Wolbachia-mediated biocontrol of West Nile virus (WNV). Ahmed et al. [27] demonstrated that environments dominated by Wolbachia significantly reduce the prevalence of WNV. Additionally, an ANN trained using LMA addresses the problem with high accuracy. Liu and Ding [28] proposed a radial basis neural network method that effectively and efficiently solves partial differential equations with high accuracy. An epidemiology model for the transmission of the mumps virus using the Mittag-Leffler Kernel was designed by Lee et al. [29], ANN was used to analyze disease dynamics.

Research studies show that the combination of FC systems and NNs can enhance the modeling of nonlinear dynamical systems and extended epidemics. Advances in highly complex computational tools and algorithms have enabled the acquisition of precise and reliable results. ANNs have been found to be effective computational tools across many applications [30–32]. FC provides a strong framework for describing and managing complex systems in science and engineering. The generalization of differentiation and integration to non-integer orders provides an efficient approach

for modeling memory effects, hereditary properties, and long-range interactions observed in various natural and applied systems. Mathematical modeling and analysis provide a structured approach for translating complex real-world problems into formal mathematical representations. Mathematics-based models facilitate the comparison of diverse infection control interventions and enhance the understanding of their epidemiological properties. Mathematical modeling is a crucial tool that enables researchers to understand complex systems and improve their decision-making.

This study presents an innovative mathematical co-infection model for HIV and HBV, along with a computational intelligence approach. The objective of this study is to obtain a numerical solution to the proposed model and analyze its dynamics. The fractional model better describes the behavior of infectious diseases in comparison to classical integer-order models, thus providing more flexibility. The Caputo derivative is very significant for the proposed model because it has a nonlocal property that includes the memory of the disease. The proposed fractional model bridges some gaps in the existing prediction models and provides a more accurate description of the HIV/HBV dynamics. This research supports data-driven policy decisions and strengthens public health initiatives to reduce HIV/HBV incidence among high-risk populations. Integrating fractional-order derivatives into disease models significantly advances epidemiological research. The results indicate a significant improvement in simulation accuracy, thereby demonstrating the value of this research. This study's main innovative contributions are:

- A novel multi-stage model for HIV/HBV coinfection is developed using Caputo's fractional derivative. This study investigates the effects of HBV immunization, evaluates recovery protocols for both asymptomatic and fully infected patients, and analyzes the incidence of secondary infections.
- A novel application of an intelligent computing solver analyzes the co-dynamics of HIV and HBV transmission. The model has two hidden layers, each with 20 neurons, and is trained using the Levenberg-Marquardt algorithm.
- Key parameters and learning dynamics of disease transmission are analyzed using a fractional-order approach to capture memory effects within the ANN. Training performance is evaluated for each compartment of the proposed model.
- The validity and reliability of the proposed ANN-LMA procedure are demonstrated using several criteria, including overlapping results, minimal absolute error, optimal training performance, regression analysis, and error histogram analysis.

This paper is structured as follows. Section 2 formulates the co-infection model. Section 3 discusses the model's basic properties, including non-negativity and boundedness. Sections 4 and 5 present the HBV-only and HIV-only sub-models, covering their equilibrium points, reproduction numbers, and stability analyses. Section 6 analyzes the sensitivity of the reproduction numbers for both diseases. Section 7 covers parameter estimation, numerical verification of theoretical results, and convergence analysis of the ANN–LMA framework. Section 8 presents the experimental analysis, network structure, results, visualizations, and discussion. Section 9 concludes with remarks on the model outcomes.

## 2. Model formulation and description

This section presents a novel mathematical framework for analyzing the dynamics of HIV and HBV co-infection within a population under the application of fractional calculus. The model utilizes a system of fractional differential equations to characterize transitions between health states over time. The population is stratified into compartments: susceptible ($S$), vaccinated for HBV ($\mathtt{V}_b$), and infection-related compartments for HBV, HIV, and their co-infection, including exposed, asymptomatic, and fully-infected states. Individuals transition between these classes through initial infection, disease progression, and recovery from HBV. The compartments $\mathtt{E}_b$, $\mathtt{E}_h$, and $\mathtt{E}_{hb}$ denote individuals who are not yet symptomatic and are exposed to HBV, HIV, or both, respectively. Entry into these compartments is governed by the force of infection from susceptible or vaccinated states, at rates $\beta_b$ for HBV and $\beta_h$ for HIV. The compartments $\mathtt{A}_b$, $\mathtt{A}_h$, and $\mathtt{A}_{hb}$ represent individuals who are infected but asymptomatic and capable of transmitting the infection. Progression from the exposed to the asymptomatic stage occurs at rates $\sigma_1$, $\sigma_2$, and $\sigma_{12}$ for HBV, HIV, and co-infection, respectively. Disease-induced death rates are denoted by $\xi_1$ for HBV, $\xi_2$ for HIV, and $\xi_{12}$ for co-infected individuals. Recovery rates for asymptomatic and infected individuals with HBV only are represented by $\theta_1$ and $\theta_2$, respectively.

The compartments $\mathtt{I}_b$, $\mathtt{I}_h$, and $\mathtt{I}_{hb}$ represent individuals fully infected with HBV, HIV, and both viruses, respectively. Two principal assumptions underlie the model: full recovery is possible only from HBV, not HIV. Consequently, individuals in the co-asymptomatic and co-infected compartments recover from HBV at rates $\theta_3$ and $\theta_4$, respectively, and subsequently transition into the asymptomatic and infected compartments of HIV only. This structure reflects the assumption that full recovery from HIV is not achievable. The compartment $R$ contains individuals who have recovered only from HBV infection. This model was previously published under the same assumptions but without including control strategies or sensitivity analysis of the reproduction numbers with respect to parameters [33]. As noted in [34], a significant proportion of acute HBV infections resolve with viral clearance or enter an inactive state, supporting the inclusion of recovery transitions in the model. Figure 1 illustrates the schematic dynamics of the fractional model.

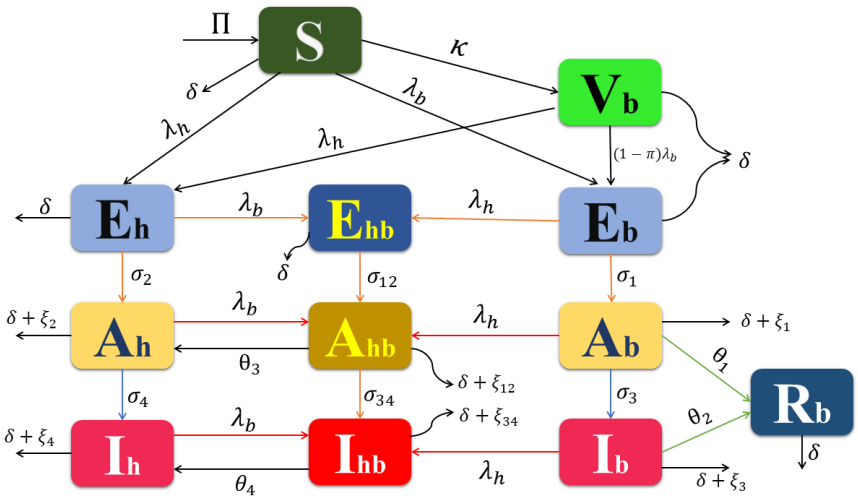


**Figure 1.** Schematic representation of the dynamic behavior of the proposed HIV/HBV model.

**Table 1.** Description of model compartments and their respective functions within the system.

| Symbol | Description |
|---|---|
| $S$ | Susceptible compartment |
| $\mathtt{V}_b$ | HBV-vaccinated individuals |
| $\mathtt{E}_b, \mathtt{E}_h, \mathtt{E}_{hb}$ | Exposed (non-infectious) individuals for each infection class |
| $\mathtt{A}_b, \mathtt{A}_h, \mathtt{A}_{hb}$ | Asymptomatic infected compartments for HBV, HIV, and co-infection |
| $\mathtt{I}_b, \mathtt{I}_h, \mathtt{I}_{hb}$ | Fully infected compartments for HBV, HIV, and co-infection |
| $\mathtt{R}_b$ | HBV recovered compartment |

The compartments of the proposed fractional model are summarized in Table 1. Public health authorities may implement targeted control measures for affected individuals in order to reduce disease transmission. The co-dynamics of HIV/HBV were analyzed using a compartmental model that divides the population into 12 distinct states. Let $T(t)$ represent the total population of this division at time t.

$$T(t) = S(t) + V_b(t) + E_b(t) + E_h(t) + E_{hb}(t) + A_b(t) + A_h(t) + A_{hb}(t) + I_b(t) + I_h(t) + I_{hb}(t) + R(t). \quad (2.1)$$

The HIV/HBV co-infection model uses Caputo's fractional derivative approach to capture nonlocal and memory effects, enhancing understanding of disease dynamics. The proposed model is governed by the following nonlinear fractional-order differential equations:

$$\begin{cases} {}^{C}D_t^{\alpha} S(t) = \Pi - (\lambda_b + \lambda_h)S - \kappa S - \delta S, \\ {}^{C}D_t^{\alpha} V_b(t) = \kappa S - (1-\pi)\,\lambda_b \mathtt{V}_b - \lambda_h \mathtt{V}_b - \delta \mathtt{V}_b, \\ {}^{C}D_t^{\alpha} E_b(t) = \lambda_b S + (1-\pi)\,\lambda_b \mathtt{V}_b - \lambda_h \mathtt{E}_b - \sigma_1 \mathtt{E}_b - \delta \mathtt{E}_b, \\ {}^{C}D_t^{\alpha} E_h(t) = \lambda_h S + \lambda_h \mathtt{V}_b - \lambda_b \mathtt{E}_h - \sigma_2 \mathtt{E}_h - \delta \mathtt{E}_h, \\ {}^{C}D_t^{\alpha} E_{hb}(t) = \lambda_h \mathtt{E}_b + \lambda_b \mathtt{E}_h - \sigma_{12} \mathtt{E}_{hb} - \delta \mathtt{E}_{hb}, \\ {}^{C}D_t^{\alpha} A_b(t) = \sigma_1 \mathtt{E}_b - \lambda_h \mathtt{A}_b - \sigma_3 \mathtt{A}_b - \theta_1 \mathtt{A}_b - (\delta + \xi_1)\,\mathtt{A}_b, \\ {}^{C}D_t^{\alpha} A_h(t) = \sigma_2 \mathtt{E}_h + \theta_3 \mathtt{A}_{hb} - \lambda_b \mathtt{A}_h - \sigma_4 \mathtt{A}_h - (\delta + \xi_2)\,\mathtt{A}_h, \\ {}^{C}D_t^{\alpha} A_{hb}(t) = \sigma_{12} \mathtt{E}_{hb} + \lambda_h \mathtt{A}_b + \lambda_b \mathtt{A}_h - \sigma_{34} \mathtt{A}_{hb} - \theta_3 \mathtt{A}_{hb} - (\delta + \xi_{12})\,\mathtt{A}_{hb}, \\ {}^{C}D_t^{\alpha} I_b(t) = \sigma_3 \mathtt{A}_b - \lambda_h \mathtt{I}_b - \theta_2 \mathtt{I}_b - (\delta + \xi_3)\,\mathtt{I}_b, \\ {}^{C}D_t^{\alpha} I_h(t) = \sigma_4 \mathtt{A}_h + \theta_4 \mathtt{I}_{hb} - \lambda_b \mathtt{I}_h - (\delta + \xi_4)\,\mathtt{I}_h, \\ {}^{C}D_t^{\alpha} I_{hb}(t) = \sigma_{34} \mathtt{A}_{hb} + \lambda_h \mathtt{I}_b + \lambda_b \mathtt{I}_h - \theta_4 \mathtt{I}_{hb} - (\delta + \xi_{34})\,\mathtt{I}_{hb}, \\ {}^{C}D_t^{\alpha} R_b(t) = \theta_1 \mathtt{A}_b + \theta_2 \mathtt{I}_b - \delta \mathtt{R}_b, \end{cases} \quad (2.2)$$

along with initial conditions

$$Y(t) \geq 0, \ \forall\, Y \in \{S, \mathtt{V}_b, \mathtt{E}_b, \mathtt{A}_b, \mathtt{I}_b, \mathtt{R}_b, \mathtt{E}_h, \mathtt{A}_h, \mathtt{I}_h, \mathtt{E}_{hb}, \mathtt{A}_{hb}, \mathtt{I}_{hb}\}, \quad (2.3)$$

where

$$\lambda_h = \beta_h \left( \frac{\mathtt{I}_h + \mathtt{I}_{hb} + \rho_3 \mathtt{A}_h + \rho_2 \mathtt{A}_{hb}}{T} \right), \quad \lambda_b = \beta_b \left( \frac{\mathtt{I}_b + \mathtt{I}_{hb} + \rho_1 \mathtt{A}_b + \rho_2 \mathtt{A}_{hb}}{T} \right), \quad (\rho_1, \rho_2, \rho_3) < 1.$$

$\lambda_b$ and $\lambda_h$ are the forces of infection for HBV and HIV, respectively, while $T$ represents the sum of all compartments. Here, $\beta_b$ and $\beta_h$ are the transmission rates for HBV and HIV, respectively, while the parameters $(\rho_1, \rho_2, \rho_3)$ modulate the transmission potential of asymptomatic individuals relative to that

of fully infectious individuals. These parameters, being less than 1, indicate reduced transmissibility in asymptomatic individuals compared with those with active symptoms. Figure 1 displays the model's transmission dynamics flowchart, while Table 1 provides a detailed description of each compartment. After adding up all the equations given in (2.2) and taking it as the change in the whole population with respect to time, we reach the following:

$$ {}^{C}D_t^{\alpha} T = \Pi - \delta T - \left(\xi_1 \mathtt{A}_b + \xi_2 \mathtt{A}_h + \xi_{12} \mathtt{A}_{hb} + \xi_3 \mathtt{I}_b + \xi_4 \mathtt{I}_h + \xi_{34} \mathtt{I}_{hb}\right). \tag{2.4} $$

## 3. Analysis of the model

This section presents the basic characteristics and analysis of the fractional model under consideration (2.2).

### *3.1. Non-negativity*

**Theorem 1.** *Let $\alpha \in (0, 1]$ and assume that the initial conditions of system (2.2) are nonnegative. Then, the solutions of the Caputo fractional-order model remain nonnegative for all $t \geq 0$, i.e.,*

$$ X(t) \in \mathbb{R}_+^{12}, \quad \forall t \geq 0, $$

where

$$ X(t) = (S, V_b, E_b, A_b, I_b, R_b, E_h, A_h, I_h, E_{hb}, A_{hb}, I_{hb}). $$

*Proof.* According to initial conditions, the proposed Caputo fractional-order model remain nonnegative for all $t \geq 0$. This condition ensures that the population variables remain biologically viable, specifically non-negative, throughout the progression of the system. We verify invariance by evaluating the system at the boundaries of each compartment. The solutions are positive, as follows:

$$ \begin{aligned}
&{}^{C}D_t^{\alpha} S(t)\,|_{S=0} = \Pi \geq 0,\\
&{}^{C}D_t^{\alpha} V_b(t)\,\big|_{V_b=0} = \kappa S \geq 0,\\
&{}^{C}D_t^{\alpha} E_b(t)\,\big|_{E_b=0} = \lambda_b S + (1-\pi)\,\lambda_b \mathtt{V}_b \geq 0,\\
&{}^{C}D_t^{\alpha} E_h(t)\,\big|_{E_h=0} = \lambda_h S + \lambda_h \mathtt{V}_b \geq 0,\\
&{}^{C}D_t^{\alpha} E_{hb}(t)\,\big|_{E_{hb}=0} = \lambda_h \mathtt{E}_b + \lambda_b \mathtt{E}_h \geq 0,\\
&{}^{C}D_t^{\alpha} A_b(t)\,\big|_{A_b=0} = \sigma_1 \mathtt{E}_b \geq 0,\\
&{}^{C}D_t^{\alpha} A_h(t)\,\big|_{A_h=0} = \sigma_2 \mathtt{E}_h + \theta_3 \mathtt{A}_{hb} \geq 0,\\
&{}^{C}D_t^{\alpha} A_{hb}(t)\,\big|_{A_{hb}=0} = \sigma_{12} \mathtt{E}_{hb} + \lambda_h \mathtt{A}_b + \lambda_b \mathtt{A}_h \geq 0,\\
&{}^{C}D_t^{\alpha} I_b(t)\,\big|_{I_b=0} = \sigma_3 \mathtt{A}_b \geq 0,\\
&{}^{C}D_t^{\alpha} I_h(t)\,\big|_{I_h=0} = \sigma_4 \mathtt{A}_h + \theta_4 \mathtt{I}_{hb} \geq 0,\\
&{}^{C}D_t^{\alpha} I_{hb}(t)\,\big|_{I_{hb}=0} = \sigma_{34} \mathtt{A}_{hb} + \lambda_h \mathtt{I}_b + \lambda_b \mathtt{I}_h \geq 0,\\
&{}^{C}D_t^{\alpha} R_b(t)\,\big|_{R_b=0} = \theta_1 \mathtt{A}_b + \theta_2 \mathtt{I}_b \geq 0.
\end{aligned} \tag{3.1} $$

Each equation shows that the derivative is non-negative on the boundary, which guarantees that the solution remains within the non-negative orthant. Therefore, all state variables remain nonnegative for all $t \geq 0$. This completes the proof.

□

*3.2. Boundedness of the model*

**Theorem 2.** *Let $\mathfrak{M}$ be the closed set defined by:*

$$\mathfrak{M} = \Big\{(S, \mathtt{V}_b, \mathtt{E}_b, \mathtt{A}_b, \mathtt{I}_b, \mathtt{R}_b, \mathtt{E}_h, \mathtt{A}_h, \mathtt{I}_h, \mathtt{E}_{hb}, \mathtt{A}_{hb}, \mathtt{I}_{hb}) \in \mathbb{R}_+^{12} : \\ S + \mathtt{V}_b + \mathtt{E}_b + \mathtt{E}_h + \mathtt{E}_{hb} + \mathtt{A}_b + \mathtt{A}_h + \mathtt{A}_{hb} + \mathtt{I}_b + \mathtt{I}_h + \mathtt{I}_{hb} + \mathtt{R}_b \leq \frac{\Pi}{\delta}\Big\}. \tag{3.2}$$

Then, the solution of the fractional-order system with Caputo derivative of order $0 < \alpha \leq 1$ remains in $\mathfrak{M}$. Hence, the set $\mathfrak{M}$ is positively invariant.

*Proof.* Let

$$T(t) = S + \mathtt{V}_b + \mathtt{E}_b + \mathtt{E}_h + \mathtt{E}_{hb} + \mathtt{A}_b + \mathtt{A}_h + \mathtt{A}_{hb} + \mathtt{I}_b + \mathtt{I}_h + \mathtt{I}_{hb} + \mathtt{R}_b.$$

Taking the Caputo fractional derivative of order $0 < \alpha \leq 1$, we obtain

$${}^{C}D_t^{\alpha} T(t) = \Pi - \delta T(t) - \Big(\xi_1 \mathtt{A}_b(t) + \xi_2 \mathtt{A}_h(t) + \xi_{12} \mathtt{A}_{hb}(t) + \xi_3 \mathtt{I}_b(t) + \xi_4 \mathtt{I}_h(t) + \xi_{34} \mathtt{I}_{hb}(t)\Big).$$

Since all parameters and state variables are non-negative, we have

$${}^{C}D_t^{\alpha} T(t) \leq \Pi - \delta T(t).$$

Thus,

$${}^{C}D_t^{\alpha} T(t) + \delta T(t) \leq \Pi.$$

Using the fractional comparison theorem, we obtain

$$T(t) \leq \frac{\Pi}{\delta} + \left(T(0) - \frac{\Pi}{\delta}\right) E_{\alpha}(-\delta t^{\alpha}),$$

where $E_{\alpha}(\cdot)$ is the Mittag–Leffler function.

Since $E_{\alpha}(-\delta t^{\alpha}) \to 0$ as $t \to \infty$, it follows that

$$T(t) \leq \frac{\Pi}{\delta}, \quad \forall t \geq 0.$$

Hence, all solutions remain in $\mathfrak{M}$, and the set $\mathfrak{M}$ is positively invariant. □

## 4. HBV only sub-model

The HBV-only sub-model is derived by assuming the absence of HIV-infected and HIV/HBV coinfected compartments. Therefore, the corresponding Caputo fractional derivatives are set to zero. ${}^{C}D_t^{\alpha} E_h = {}^{C}D_t^{\alpha} A_h = {}^{C}D_t^{\alpha} I_h = {}^{C}D_t^{\alpha} E_{hb} = {}^{C}D_t^{\alpha} A_{hb} = {}^{C}D_t^{\alpha} I_{hb} = 0$ . Thus, we have the following dynamical system:

$$\begin{cases} {}^{C}D_t^{\alpha} S(t) = \Pi - (\lambda_b + \kappa + \delta)S, \\ {}^{C}D_t^{\alpha} V_b(t) = \kappa S - (1-\pi)\,\lambda_b \mathtt{V}_b - \delta \mathtt{V}_b, \\ {}^{C}D_t^{\alpha} E_b(t) = \lambda_b S + (1-\pi)\,\lambda_b \mathtt{V}_b - \sigma_1 \mathtt{E}_b - \delta \mathtt{E}_b, \\ {}^{C}D_t^{\alpha} A_b(t) = \sigma_1 \mathtt{E}_b - \sigma_3 \mathtt{A}_b - \theta_1 \mathtt{A}_b - (\delta + \xi_1)\,\mathtt{A}_b, \\ {}^{C}D_t^{\alpha} I_b(t) = \sigma_3 \mathtt{A}_b - \theta_2 \mathtt{I}_b - (\delta + \xi_3)\,\mathtt{I}_b, \\ {}^{C}D_t^{\alpha} R_b(t) = \theta_1 \mathtt{A}_b + \theta_2 \mathtt{I}_b - \delta \mathtt{R}_b, \end{cases} \tag{4.1}$$

where

$$\lambda_b = \beta_b \left( \frac{\mathtt{I}_b + \rho_1 \mathtt{A}_b}{T_B} \right), T_B = S(t) + \mathtt{V}_b(t) + \mathtt{E}_b(t) + \mathtt{A}_b(t) + \mathtt{I}_b(t) + \mathtt{R}_b(t).$$

### *4.1. Equilibrium points*

The model's equilibrium points (4.1) are given in this subsection. $\mathtt{F}^0$ represents the absence of disease, whereas $\mathtt{F}^*$ represents the presence of sickness.

$$\mathtt{F}^0 = \left( S^0, \mathtt{V}_b^0, \mathtt{E}_b^0, \mathtt{A}_b^0, \mathtt{I}_b^0, \mathtt{R}_b^0 \right) = \left( \frac{\Pi}{\kappa + \delta}, \frac{\kappa \Pi}{\delta(\kappa + \delta)}, 0, 0, 0, 0 \right). \tag{4.2}$$

$$\mathtt{F}^* = \left( S^*, \mathtt{V}_b^*, \mathtt{E}_b^*, \mathtt{A}_b^*, \mathtt{I}_b^*, \mathtt{R}_b^* \right),$$

where

$$\begin{aligned} S^* &= \frac{\Pi}{\lambda_b + \delta + \kappa}, \ \mathtt{V}_b^* = \frac{\kappa \Pi}{(\lambda_b + \delta + \kappa)(\delta + \lambda_b(1-\pi))}, \\ \mathtt{E}_b^* &= \frac{\lambda_b \Pi(\lambda_b(1-\pi) + \delta + \kappa + \kappa\pi)}{k_1(\lambda_b + \delta + \kappa)(\lambda_b(1-\pi) + \delta)}, \ \mathtt{A}_b^* = \frac{\sigma_1 \lambda_b \Pi(\lambda_b(1-\pi) + \delta + \kappa + \kappa\pi)}{k_1 k_4(\lambda_b + \delta + \kappa)(\lambda_b(1-\pi) + \delta)}, \\ \mathtt{I}_b^* &= \frac{\sigma_1 \sigma_3 \lambda_b \Pi(\lambda_b(1-\pi) + \delta + \kappa + \kappa\pi)}{k_1 k_4 k_7(\lambda_b + \delta + \kappa)(\lambda_b(1-\pi) + \delta)}, \ \mathtt{R}_b^* = \frac{\sigma_1 \lambda_b \Pi(\lambda_b(1-\pi) + \delta + \kappa + \kappa\pi)(\sigma_3\theta_2 + \theta_1 k_7)}{k_1 k_4 k_7 \delta(\lambda_b + \delta + \kappa)(\lambda_b(1-\pi) + \delta)}, \end{aligned} \tag{4.3}$$

where

$$k_1 = \sigma_1 + \delta, \quad k_4 = \sigma_3 + \theta_1 + \delta + \xi_1, \quad k_7 = \theta_2 + \delta + \xi_3.$$

The endemic equilibrium is both present and epidemiologicaly relevant when the associated basic reproduction number is greater than one (i.e., $R_B > 1$).

### *4.2. Reproduction number*

The reproduction number of model (4.1) is calculated by using the next-generation approach [35].

$$F = \begin{bmatrix} 0 & \frac{\beta_b \rho_1}{T_B^0}(S^0 + (1-\pi)V_B^0) & \frac{\beta_b}{T_B^0}(S^0 + (1-\pi)V_B^0) \\ 0 & 0 & 0 \\ 0 & 0 & 0 \end{bmatrix}, \ V = \begin{bmatrix} k_1 & 0 & 0 \\ -\sigma_1 & k_4 & 0 \\ 0 & -\sigma_3 & k_7 \end{bmatrix},$$

$$FV^{-1} = \begin{bmatrix} \frac{(\delta - \pi\kappa + \kappa)\sigma_1\sigma_3\beta_b}{(\delta+\kappa)k_1k_4k_7} + \frac{(\delta - \pi\kappa + \kappa)\sigma_1\rho_1\beta_b}{(\delta+\kappa)k_1k_4} & \frac{(\delta - \pi\kappa + \kappa)\sigma_3\beta_b}{(\delta+\kappa)k_4k_7} + \frac{(\delta - \pi\kappa + \kappa)\rho_1\beta_b}{(\delta+\kappa)k_4} & \frac{(\delta - \pi\kappa + \kappa)\beta_b}{(\delta+\kappa)k_7} \\ 0 & 0 & 0 \\ 0 & 0 & 0 \end{bmatrix},$$

$$R_B = \frac{\sigma_1 \beta_b \left(\sigma_3 + \rho_1 k_7\right)\left(\delta + \kappa(1-\pi)\right)}{k_1 k_4 k_7 (\delta + \kappa)}. \tag{4.4}$$

*4.3. Local stability*

**Theorem 3.** *The state presenting the absence of disease* $\mathrm{F}^0$ *is locally asymptotically stable (LAS) if* $R_B < 1$ *and unstable if* $R_B > 1$.

*Proof.* The Routh-Hurwitz approach is implemented to demonstrate the model's local stability (4.1). Let us begin by calculating the system's Jacobian (4.1) at $\mathrm{F}^0$. We get the following matrix:

$$J(\mathrm{F}^0) = \begin{bmatrix} -(\kappa+\delta) & 0 & 0 & -\frac{\beta_b\rho_1\delta}{\delta+\kappa} & -\frac{\beta_b\delta}{\delta+\kappa} & 0 \\ \kappa & -\delta & 0 & -\frac{\beta_b\rho_1\kappa(1-\pi)}{\delta+\kappa} & -\frac{\beta_b\kappa(1-\pi)}{\delta+\kappa} & 0 \\ 0 & 0 & -k_1 & \frac{\beta_b\rho_1(\delta+\kappa(1-\pi))}{\delta+\kappa} & \frac{\beta_b(\delta+\kappa(1-\pi))}{\delta+\kappa} & 0 \\ 0 & 0 & \sigma_1 & -k_4 & 0 & 0 \\ 0 & 0 & 0 & \sigma_3 & -k_7 & 0 \\ 0 & 0 & 0 & \theta_1 & \theta_2 & -\delta \end{bmatrix}.$$

The above matrix has the following characteristic equation:

$$\begin{aligned} &\frac{1}{\delta+\kappa}(\lambda+\delta)^2(\lambda+\delta+\kappa)(\lambda^3(\delta+\kappa)+k_7\lambda^2\delta+k_7\lambda^2\kappa \\ &+k_4\lambda\left(\lambda+k_7\right)(\delta+\kappa)+k_1\left(\lambda+k_4\right)\left(\lambda+k_7\right)(\delta+\kappa) \\ &-\sigma_1\beta_b\rho_1\left(\lambda+k_7\right)(\delta+\kappa-\kappa\pi)-\sigma_1\sigma_3\beta_b\delta-\sigma_1\sigma_3\beta_b\kappa+\sigma_1\sigma_3\beta_b\kappa\pi)=0. \end{aligned} \tag{4.5}$$

The model's first three eigenvalues

$$\lambda_1, = -\delta(twice),\ \lambda_2 = -(\delta+\kappa).$$

The remaining part of Eq (4.5) is

$$\lambda^3 + \mathbf{a_1}\lambda^2 + \mathbf{a_2}\lambda + \mathbf{a_3} = 0,$$

where

$$\mathbf{a_1} = k_1 + k_4 + k_7, \quad \mathbf{a_3} = k_1k_4k_7(1-R_B), \quad \mathbf{a_2} = k_1k_7 + k_4k_7 + \frac{\beta_b\sigma_1\sigma_3(\delta+\kappa(1-\pi))}{k_7(\delta+\kappa)} + k_1k_4(1-R_B).$$

As revealed by the equation, the coefficient $\mathbf{a_1}$ carries a positive sign. Meanwhile, the values of $\mathbf{a_2}$ and $\mathbf{a_3}$ are influenced by $R_B$, and, notably, these coefficients also become positive when $R_B$ falls below 1. Substituting the parameter values from Table 2, we obtain the following: $a_1 \approx 1.2036$, $a_2 \approx 0.4085$, $a_3 \approx 0.0370$. Hence, $a_1a_2 \approx 0.4917 > 0.0370 \approx a_3$.

Therefore, the Routh–Hurwitz condition $a_1a_2 > a_3$ is satisfied. Since $a_1 > 0$, $a_2 > 0$, and $a_3 > 0$ whenever $R_B < 1$, all the eigenvalues of the characteristic polynomial have negative real parts. This aligns with the Routh-Hurwitz criterion [36], which states that the model in question, denoted as (4.1), exhibits locally asymptotic stability (LAS) under the condition that $R_B$ remains less than 1. □

**Table 2.** Model parameters and their biological descriptions.

| Symbol | Description | Values | Units | Reference |
|---|---|---|---|---|
| $\Pi$ | Recruitment rate into susceptible population | 569000/81 | 1/year | [39] |
| $\delta$ | Natural death rate | 1/81 | 1/year | [39] |
| $\beta_b$ | HBV transmission rate | 0.1692 | 1/year | [33] |
| $\beta_h$ | HIV transmission rate | 0.2055 | 1/year | [33] |
| $\kappa$ | progress rate of susceptible individuals to HBV vaccinated class | 0.4399 | 1/year | [33] |
| $\sigma_1$ | Rate of progression from exposed to asymptomatic for HBV | 0.1989 | 1/year | estimated |
| $\sigma_2$ | Rate of progression from exposed to asymptomatic for HIV | 0.2369 | 1/year | estimated |
| $\pi$ | Proportion of individuals successfully vaccinated against HBV | 0.4399 | Dimensionless | assumed |
| $\sigma_{12}$ | Rate of progression from exposed to asymptomatic for co-infection | 0.35 | 1/year | assumed |
| $\sigma_3$ | Rate of progression from asymptomatic to fully infected for HBV | 0.2357 | 1/year | estimated |
| $\sigma_4$ | Rate of progression from asymptomatic to fully infected for HIV | 0.1520 | 1/year | estimated |
| $\sigma_{34}$ | Rate of progression from asymptomatic to fully infected for co-infection | 0.22 | 1/year | assumed |
| $\theta_1$ | Recovery rate of asymptomatic individuals from HBV | 0.23 | 1/year | assumed |
| $\theta_2$ | Recovery rate of infected individuals from HBV | 0.27 | 1/year | fitted |
| $\theta_3$ | Recovery rate of co-asymptomatic individuals from HBV | 0.15 | 1/year | assumed |
| $\theta_4$ | Recovery rate of co-infected individuals from HBV | 0.16 | 1/year | assumed |
| $\xi_1$ | Disease-induced death rate for HBV asymptomatic individuals | 0.222 | 1/year | fitted |
| $\xi_2$ | Disease-induced death rate for HIV asymptomatic individuals | 0.2 | 1/year | fitted |
| $\xi_{12}$ | Disease-induced death rate for co-asymptomatic individuals | 0.15 | 1/year | fitted |
| $\xi_3$ | Disease-induced death rate for HBV infected individuals | 0.01 | 1/year | [41] |
| $\xi_4$ | Disease-induced death rate for HIV infected individuals | 0.333 | 1/year | [41] |
| $\xi_{34}$ | Disease-induced death rate for co-infected individuals | 0.001 | 1/year | [41] |
| $\rho_1$ | Relative infectiousness of asymptomatic HBV individuals compared to symptomatic HBV-infected individuals | 0.3 | Dimensionless | assumed |
| $\rho_2$ | Relative infectiousness of asymptomatic HBV–HIV co-infected individuals | 0.18 | Dimensionless | assumed |
| $\rho_3$ | Relative infectiousness of asymptomatic HIV individuals | 0.25 | Dimensionless | assumed |

## 5. HIV only sub-model

The HIV-only sub-model is derived by assuming the absence of HBV-infected and HIV/HBV coinfected compartments. As a result, the corresponding Caputo fractional derivatives are set to zero. ${}^{C}D_t^{\alpha}V_b = {}^{C}D_t^{\alpha}E_b = {}^{C}D_t^{\alpha}A_b = {}^{C}D_t^{\alpha}I_b = {}^{C}D_t^{\alpha}E_{hb} = {}^{C}D_t^{\alpha}A_{hb} = {}^{C}D_t^{\alpha}I_{hb} = 0$. Consequently, we have the dynamical system that follows:

$$\begin{cases} {}^{C}D_t^{\alpha} S(t) = \Pi - \lambda_h S - \delta S, \\ {}^{C}D_t^{\alpha} E_h(t) = \lambda_h S - \sigma_2 \mathtt{E}_h - \delta \mathtt{E}_h, \\ {}^{C}D_t^{\alpha} A_h(t) = \sigma_2 \mathtt{E}_h - \sigma_4 \mathtt{A}_h - (\delta + \xi_2)\, \mathtt{A}_h, \\ {}^{C}D_t^{\alpha} I_h(t) = \sigma_4 \mathtt{A}_h - (\delta + \xi_4)\, \mathtt{I}_h. \end{cases} \tag{5.1}$$

where

$$\lambda_h = \beta_h \left( \frac{\mathtt{I}_h + \rho_3 \mathtt{A}_h}{T_H} \right), T_H = S(t) + \mathtt{E}_h(t) + \mathtt{A}_h(t) + \mathtt{I}_h(t)$$

is the force of infection of HIV.

### *5.1. Equilibrium points*

Similar to what we accomplished with the model that was mentioned earlier, we also estimated equilibrium points for the HIV-only model.

$$\mathtt{F}^0 = \left( S^0, \mathtt{E}_h^0, \mathtt{A}_h^0, \mathtt{I}_h^0 \right) = \left( \frac{\Pi}{\delta}, 0, 0, 0 \right). \tag{5.2}$$

The point at which the disease is present is shown by

$$\mathtt{F}^* = \left( S^*, \mathtt{E}_h^*, \mathtt{A}_h^*, \mathtt{I}_h^* \right),$$

where

$$S^* = \frac{\Pi}{\lambda_h + \delta},\ \mathtt{E}_h^* = \frac{\lambda_h \Pi}{k_2(\lambda_h + \delta)},\ \mathtt{A}_h^* = \frac{\sigma_2 \lambda_h \Pi}{k_2 k_5 (\lambda_h + \delta)},\ \mathtt{I}_h^* = \frac{\sigma_2 \sigma_4 \lambda_h \Pi}{k_2 k_5 k_8 (\lambda_h + \delta)}, \tag{5.3}$$

and

$$k_2 = \sigma_2 + \delta, \quad k_5 = \sigma_4 + \delta + \xi_2, \quad k_8 = \delta + \xi_4.$$

The endemic equilibrium is both present and epidemiologically relevant when the associated basic reproduction number is greater than one (i.e., $R_H > 1$).

### *5.2. Reproduction number*

To determine the reproduction number for the HIV sub-model, a methodology analogous to that used for calculating the HBV reproduction number is employed [37], as outlined in Eq (5.1).

$$F = \begin{bmatrix} 0 & \beta_h \rho_3 & \beta_h \\ 0 & 0 & 0 \\ 0 & 0 & 0 \end{bmatrix},\ V = \begin{bmatrix} k_2 & 0 & 0 \\ -\sigma_2 & k_5 & 0 \\ 0 & -\sigma_4 & k_8 \end{bmatrix},\ FV^{-1} = \begin{bmatrix} \frac{\sigma_2 \sigma_4 \beta_h}{k_2 k_5 k_8} + \frac{\sigma_2 \rho_3 \beta_h}{k_2 k_5} & \frac{\sigma_4 \beta_h}{k_5 k_8} + \frac{\rho_3 \beta_h}{k_5} & \frac{\beta_h}{k_8} \\ 0 & 0 & 0 \\ 0 & 0 & 0 \end{bmatrix},$$

$$R_H = \frac{\sigma_2 \beta_h (\sigma_4 + \rho_3 k_8)}{k_2 k_5 k_8}. \tag{5.4}$$

*5.3. Local stability*

**Theorem 4.** *The state when the disease is not present, as demonstrated by* $\mathrm{F}^0$ *of the model (5.1), is LAS if* $R_H < 1$ *and unstable if* $R_H > 1$.

*Proof.*

$$J(\mathrm{F}^0) = \begin{bmatrix} -\delta & 0 & -\beta_h\rho_3 & -\beta_h \\ 0 & -k_2 & \beta_h\rho_3 & \beta_h \\ 0 & \sigma_2 & -k_5 & 0 \\ 0 & 0 & \sigma_4 & -k_8 \end{bmatrix}.$$

$$(-\lambda - \delta)\left(\sigma_2\sigma_4\beta_h + (\sigma_2\beta_h\rho_3 - (\lambda + k_2)(\lambda + k_5))\right)(\lambda + k_8) = 0. \tag{5.5}$$

$$\lambda_1 = -\delta.$$

As a result, let us discuss the equation taken from (5.5).

$$\lambda^3 + \mathbf{b_1}\lambda^2 + \mathbf{b_2}\lambda + \mathbf{b_3} = 0,$$

where

$$\mathbf{b_1} = k_2 + k_5 + k_8, \quad \mathbf{b_2} = k_8(k_2 + k_5) + \frac{\beta_h\sigma_2\sigma_4}{k_8} + k_2k_5(1 - R_H), \quad \mathbf{b_3} = k_2k_5k_8(1 - R_H).$$

The equation shows that $\mathbf{b_1}$ is positive. The other coefficients, $\mathbf{b_2}$ and $\mathbf{b_3}$, have an impact on the value of $R_H$. These coefficients are positive when $R_H < 1$. Substituting the parameter values from Table 2, we obtain $b_1 \approx 0.9589$, $b_2 \approx 0.2905$, and $b_3 \approx 0.0198$. Hence, $b_1b_2 \approx 0.2786 > 0.0198 \approx b_3$. Therefore, the Routh–Hurwitz condition $b_1b_2 > b_3$ holds. Since $b_1 > 0$, $b_2 > 0$, and $b_3 > 0$ whenever $R_H < 1$, all eigenvalues have negative real parts. Thus, the disease-free equilibrium is locally asymptotically stable whenever $R_H < 1$. □

## 6. Sensitivity analysis of $R_B$ and $R_H$

In this section, we conduct a sensitivity analysis to investigate potential hidden effects of multiple related parameters on the reproduction numbers in the co-infection model. The primary aim of this study is to identify the parameters that can substantially affect the models' results, even with minor numerical changes. To accomplish this objective, a defined methodology is employed: modifying parameter input values to observe the resulting variations in the output. We combined Latin hypercube sampling (LHS) with partial rank correlation coefficients (PRCC) to conduct a sensitivity analysis assessing how model parameters affect reproduction numbers and transmission dynamics. To ensure that the input space is adequately covered, we employed 1000 parameter sets from biologically relevant ranges. For measuring the strength and the nature of the influence exerted by each parameter, we applied PRCC analysis. This technique highlights those parameters that play the largest role in spreading co-infections, and takes into account the non-linearity between the parameters. The simulations were conducted using MATLAB R2024a. The PRCC-based sensitivity analysis results for reproduction numbers $R_h$ and $R_b$ are depicted in Figure 2. The results for the PRCC values of the

model parameters are displayed in Figure 2(a). The parameter $\beta_h$ has the strongest positive influence on $R_h$ because its PRCC value is 0.98. From the graph above, it can be observed that the reproduction number is affected greatly by changes in the transmission rate. Furthermore, from the PRCC value of 0.89, the parameter $\rho_3$ has been found to be highly positively correlated with $R_h$. On the other hand, the sensitivity value of $\sigma_4$ is 0.70. The parameter $\sigma_2$ has a PRCC value of 0.34, which means it has a small positive effect. On the other hand, the parameters $\xi_4$ and $\xi_2$ have high negative correlations with PRCC values of $-0.96$ and $-0.95$, respectively. This means that raising these parameters lowers the value of $R_h$. The parameter $\delta$ also has a negative effect on the response variable, with a PRCC of $-0.55$, indicating a moderate inverse association. Figure 2(b) shows the PRCC values of the model parameters in relation to $R_b$. The parameter $\beta_b$ has a strong positive relationship with a PRCC value of 0.89, which means that when the transmission rate goes up, $R_b$ also goes up. The factors $\sigma_1$ and $\sigma_3$ show positive impacts with PRCC values of 0.21 and 0.55, respectively. $\rho_1$ shows a moderate positive effect with a value of 0.41. On the other hand, some parameters show negative sensitivity. The parameter $\pi$ shows the largest negative correlation with a PRCC value of $-0.96$, and $\theta_2$ comes in second with $-0.77$. The parameters $\theta_1$ and $\delta$ exhibit negative correlations of $-0.55$ and $-0.29$, respectively. Likewise, $\xi_1$, $\kappa$, and $\xi_3$ exhibit diminished negative contributions, with PRCC values of $-0.58$, $-0.18$, and $-0.06$, respectively.

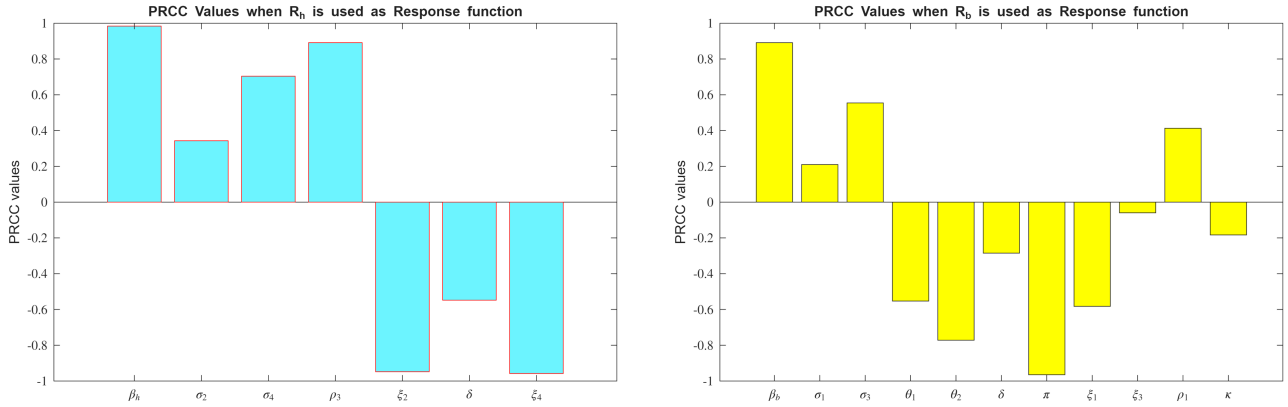


**(a)** PRCC values for $R_h$.

**(b)** PRCC values for $R_b$.

**Figure 2.** Sensitivity analysis of $R_h$ and $R_b$ using PRCC values.

Figure 3 presents sensitivity analysis of the reproduction numbers $R_h$ and $R_b$ through regression plots. Figure 3(a) presents regression plots for all the parameters with respect to $R_h$. The fitted regression lines on the scatter distributions support the sensitivity results obtained from the PRCC analysis. The PRCC values for the parameters $\beta_h$, $\sigma_2$, $\sigma_4$, and $\rho_3$ are 0.98, 0.34, 0.70, and 0.89, respectively. These values show positive regression trends. The parameters $\xi_2$, $\delta$, and $\xi_4$ exhibit negative regression trends, with PRCC values of $-0.95$, $-0.55$, and $-0.96$, respectively. Increasing these parameter values reduces $R_h$. Figures 3(b) and 3(c) present regression relationships $R_b$ and the corresponding parameters of the sensitivity analysis of the reproduction number $R_b$ using PRCC indices and regression plots. The fitted regression lines for $\beta_b$, $\sigma_1$, $\sigma_3$, and $\rho_1$ show upward trends, consistent with their positive PRCC indices. In contrast, the parameters $\theta_1$, $\theta_2$, $\delta$, $\pi$, $\xi_1$, $\kappa$, and $\xi_3$ exhibit declining regression patterns, consistent with their negative PRCC values. The significant decrease is observed for $\pi$ and $\theta_2$ highlights their greater influence on reducing $R_b$, while the other parameters exhibit

comparatively weaker effects. In general, sensitivity analysis shows that the transmission parameters have a considerable impact on the number of reproductions. As a conclusion, $\beta_h$ and $\beta_b$ have strong positive relationships with $R_h$ and $R_b$, respectively. This means that the disease spreads much faster when the transmission rates are higher. Negative correlation is observed for variables such as $\pi$, $\xi_2$, $\xi_4$, and $\theta_2$. This implies that increasing values of these parameters lead to decreased reproduction numbers. The results presented in the regression plots confirm the impact of the identified parameters. The obtained results provide an insight into the most influential parameters within the model and the importance of these parameters in the prevention of the disease spread.

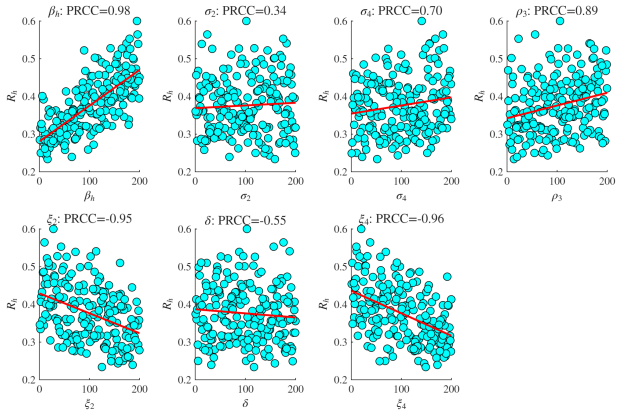


**(a)** Regression plot for $R_h$.

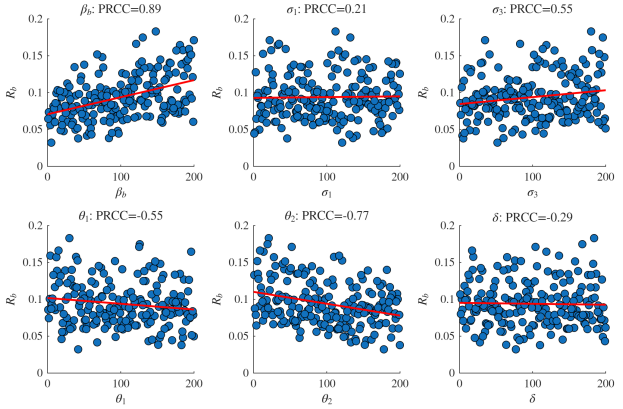


**(b)** Regression plot for $R_b$ (Part I).

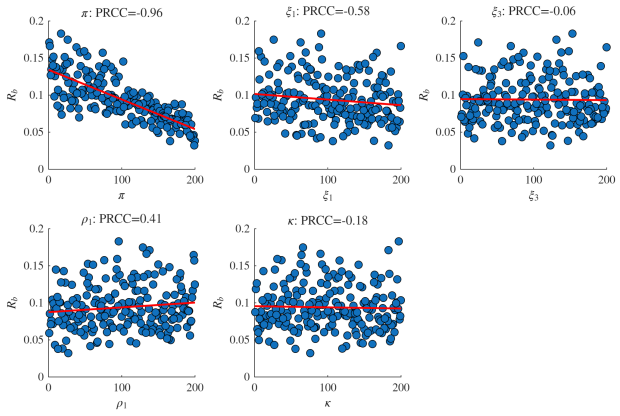


**(c)** Regression plot for $R_b$ (Part II).

**Figure 3.** PRCC-values-based sensitivity analysis of $R_b$ and $R_h$ through regression plots.

## 7. Parameter estimation

The nonlinear least-squares regression curve-fitting technique is applied to estimate model parameters, as described in a previous study [33]. We use the "fmincon" function in MATLAB to fit the data for the proposed coinfection model. It initially establishes parameters and initializes cumulative coinfection HIV/HBV data spanning 23 years in Taiwan. Subsequently, we designed an objective function that minimized the discrepancy between reported data and model estimates. This

study focuses on model parameter estimation and data fitting for the proposed coinfection model. The modeling is performed through MATLAB R2024a. The annually estimated HIV/HBV coinfection series derived from a previous study [33] and further calibrated using Taiwan HIV/AIDS surveillance records from the Centers for Disease Control (CDC) [38]. Population data were obtained from Worldometer [39, 40]. As our previous study [33] provides a detailed account of the parameter estimation procedure, we offer only a concise overview here.

The parameter values in Table 2 were determined by fitting the model to estimated data. This estimation improves the accuracy and predictive capability of the co-infection model.

Figure 4(a) presents estimated trends of the HIV/HBV coinfection model. Figure 4(b) shows the calibrated model's fit to the estimated data. Table 2 summarizes the estimated and assumed parameter values used in the simulation. Figure 5 illustrates the proposed ANN-LMA framework, which includes two hidden layers with 20 neurons each and one output layer.

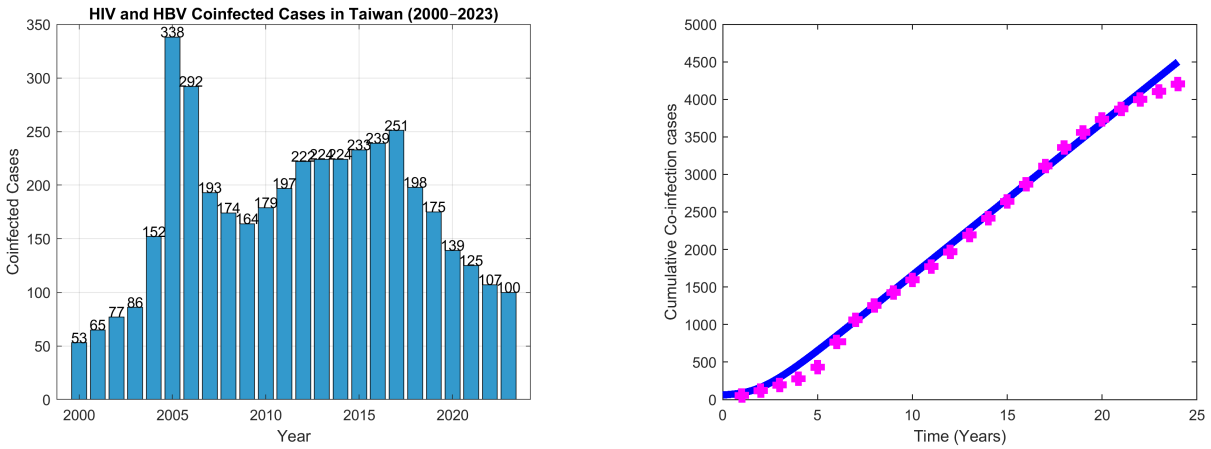


**(a)** Estimated HIV/HBV coinfection series [33].. **(b)** Model fitting curve against estimated data.

**Figure 4.** Curve fitting through estimated data.

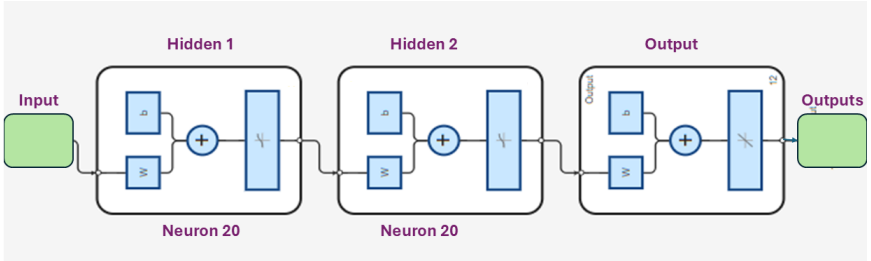


**Figure 5.** Architecture of the proposed artificial neural networks (ANNs).

### *7.1. Numerical verification and convergence analysis*

In this section, we numerically verify the theoretical properties of the proposed HIV/HBV coinfection model and evaluate the performance of the ANN–LMA computational framework. We validate the theoretical findings related to the positivity, boundedness, and stability properties of the solutions to the considered model via numerical simulations. Besides, the ANN-LMA algorithm is

assessed based on various metrics such as MSE, RMSE, gradient measures, error histograms, fitness plots, and regression analysis. Table 3 summarizes the convergence and stability analysis of the proposed ANN-LMA computational framework.

**Table 3.** Statistical results of ANNs-LMA.

| Compartments | Mean square error | | | MSE | RMSE | Gradient | Mu | cpu time |
|---|---|---|---|---|---|---|---|---|
| | Training | Testing | Testing | | | | | (sec.) |
| $S(t)$ | 5.43E-9 | 1.38E-9 | 8.54E-9 | 1.38E-9 | 3.71E-5 | 0.00184 | 1.00e-06 | 19 |
| $V_b(t)$ | 1.66E-11 | 2.64E-11 | 2.35E-11 | 2.64E-11 | 5.14E-5 | 0.000909 | 1.00e-09 | 67 |
| $E_b(t)$ | 7.59E-8 | 1.31E-7 | 1.01E-7 | 1.31E-7 | 3.62E-4 | 0.00218 | 1.00e-05 | 17 |
| $E_h(t)$ | 6.51E-11 | 2.95E-10 | 2.15E-9 | 2.95E-10 | 1.72E-5 | 0.00270 | 1.00e-08 | 26 |
| $E_{hb(t)}$ | 6.09E-10 | 2.42E-9 | 7.49E-10 | 2.42E-9 | 4.92E-5 | 0.00263 | 1.00e-07 | 18 |
| $A_b(t)$ | 4.35E-8 | 7.04E-8 | 8.54E-9 | 7.04E-8 | 2.80E-4 | 0.00776 | 1.00e-05 | 18 |
| $A_h(t)$ | 7.60E-9 | 5.14E-8 | 8.54E-9 | 5.14E-8 | 2.27E-4 | 0.00124 | 1.00e-06 | 28 |
| $A_{hb(t)}$ | 2.04E-11 | 1.11E-10 | 1.77E-10 | 1.11E-10 | 1.05E-5 | 1.7e-05 | 1.00e-08 | 10 |
| $I_b(t)$ | 1.12E-9 | 1.25E-6 | 1.948E-6 | 1.25E-6 | 1.10E-3 | 0.00285 | 0.001 | 17 |
| $I_h(t)$ | 6.26E-12 | 8.33E-12 | 8.18E-12 | 8.33E-12 | 2.88E-6 | 0.00290 | 1.00e-09 | 18 |
| $I_{hb(t)}$ | 7.78E-9 | 1.36E-8 | 7.94E-9 | 1.36E-8 | 1.16E-4 | 0.00146 | 1.00e-06 | 17 |
| $R_b(t)$ | 9.68E-10 | 1.43E-9 | 2.27E-9 | 1.43E-9 | 3.78E-5 | 0.00234 | 1.00e-07 | 16 |

### *7.2. Numerical verification of theoretical results*

To verify the analytical results established in the theoretical section, numerical simulations were conducted using the parameter values listed in Table 3. Throughout the entire simulation interval, all state variables remained non-negative, thereby confirming the positivity result demonstrated in Theorem 3.1. No compartment exhibited negative values during the simulations, which supports the biological feasibility of the proposed HIV/HBV coinfection model. Furthermore, the numerical simulations corroborate the theoretical boundedness result, as all solutions remain within the biologically feasible region described in Theorem 3.2. According to the theoretical analysis, the viable region is defined by

$$\Omega = \left\{ N(t) \leq \frac{\Pi}{\delta} \right\}.$$

Using the demographic parameters,

$$\frac{\Pi}{\delta} = \frac{569000/81}{1/81} = 569000.$$

The total population remained below the specified threshold throughout the simulation period. This finding supports the boundedness theorem and confirms that all solutions are within the biologically relevant domain. Furthermore, the estimated parameter values facilitated the calculation of threshold parameters for the HIV and HBV sub-models. The HIV reproduction number was estimated as $R_H = 0.370$, and the HBV reproduction number as $R_B = 0.144$.

Because both reproduction numbers satisfy $R_H < 1$ and $R_B < 1$, the disease-free equilibrium is locally asymptotically stable according to established stability theorems. In alignment with these

theoretical predictions, the infected compartments declined toward zero in the numerical simulations. These numerical results corroborate the analytical findings and further confirm the validity of the positivity, boundedness, and local stability properties of the proposed model.

## 8. Results and discussion: experimental analysis with artificial neural networks

This section examines the application of ANNs employing LMA, supported by significant experimental findings and an in-depth analysis. An innovative application of the intelligent computing solution ANN-LMA is presented to examine the co-dynamics of HIV and HBV, taking into account the impacts of HBV vaccination, as well as exposed and asymptomatic transmission. This analysis employs two hidden layers, each including 20 neurons, and is trained via the LMA method. The mathematical expressions for the proposed ANNs are presented below.

$$\mathbf{L}^{(1)} = \begin{bmatrix} L_1^{(1)} \\ L_2^{(1)} \\ L_3^{(1)} \\ L_4^{(1)} \\ \vdots \\ L_{20}^{(1)} \end{bmatrix} = \Gamma\left(\begin{bmatrix} \omega_{1,1}^{(1)} \\ \omega_{2,1}^{(1)} \\ \omega_{3,1}^{(1)} \\ \omega_{4,1}^{(1)} \\ \vdots \\ \omega_{20,1}^{(1)} \end{bmatrix} t + \begin{bmatrix} b_1^{(1)} \\ b_2^{(1)} \\ b_3^{(1)} \\ b_4^{(1)} \\ \vdots \\ b_{20}^{(1)} \end{bmatrix}\right), \tag{8.1}$$

$$\mathbf{L}^{(2)} = \begin{bmatrix} L_1^{(2)} \\ L_2^{(2)} \\ L_3^{(2)} \\ L_4^{(2)} \\ \vdots \\ L_{20}^{(2)} \end{bmatrix} = \Gamma\left(\begin{bmatrix} \omega_{1,1}^{(2)} & \omega_{1,2}^{(2)} & \cdots & \omega_{1,20}^{(2)} \\ \omega_{2,1}^{(2)} & \omega_{2,2}^{(2)} & \cdots & \omega_{2,20}^{(2)} \\ \omega_{3,1}^{(2)} & \omega_{3,2}^{(2)} & \cdots & \omega_{3,20}^{(2)} \\ \omega_{4,1}^{(2)} & \omega_{4,2}^{(2)} & \cdots & \omega_{4,20}^{(2)} \\ \vdots & \vdots & \ddots & \vdots \\ \omega_{20,1}^{(2)} & \omega_{20,2}^{(2)} & \cdots & \omega_{20,20}^{(2)} \end{bmatrix} \begin{bmatrix} L_1^{(1)} \\ L_2^{(1)} \\ L_3^{(1)} \\ L_4^{(1)} \\ \vdots \\ L_{20}^{(1)} \end{bmatrix} + \begin{bmatrix} b_1^{(2)} \\ b_2^{(2)} \\ b_3^{(2)} \\ b_4^{(2)} \\ \vdots \\ b_{20}^{(2)} \end{bmatrix}\right), \tag{8.2}$$

$$\begin{bmatrix} S(t) \\ V_b(t) \\ E_b(t) \\ E_h(t) \\ \vdots \\ R_b(t) \end{bmatrix} = \begin{bmatrix} w_{1,1}^{(3)} & w_{1,2}^{(3)} & \cdots & w_{1,20}^{(3)} \\ w_{2,1}^{(3)} & w_{2,2}^{(3)} & \cdots & w_{2,20}^{(3)} \\ w_{3,1}^{(3)} & w_{3,2}^{(3)} & \cdots & w_{3,20}^{(3)} \\ w_{4,1}^{(3)} & w_{4,2}^{(3)} & \cdots & w_{4,20}^{(3)} \\ \vdots & \vdots & \ddots & \vdots \\ w_{12,1}^{(3)} & w_{12,2}^{(3)} & \cdots & w_{12,20}^{(3)} \end{bmatrix} \begin{bmatrix} L_1^{(2)} \\ L_2^{(2)} \\ L_3^{(2)} \\ L_4^{(2)} \\ \vdots \\ L_{20}^{(2)} \end{bmatrix} + \begin{bmatrix} B_1 \\ B_2 \\ B_3 \\ B_4 \\ \vdots \\ B_{12} \end{bmatrix}, \tag{8.3}$$

where

- $\omega^{(1)}$, $\omega^{(2)}$, and $w^{(3)}$ are weights,
- $b^{(1)}$ , ($b^{(2)}$), and $B$ are biases,
- $\Gamma$ is the sigmoid activation function.

$$\sigma(t) = \frac{1}{1 + e^{-t}}. \tag{8.4}$$

The number of neurons is chosen based on a thorough analysis. Too many neurons can cause

overfitting, while too few can cause convergence before training and underfitting. In this work, the log-sigmoid activation function is used to map real-valued inputs to output values ranging from 0 to 1. The log-sigmoid function is widely used in neural networks, and it is especially useful for the output layer in neural networks used in binary classification and logistic regression. The mathematical formula of the log-sigmoid function is presented in Equation (8.4). The log-sigmoid function is always a differentiable function, and therefore, it is possible to use it in gradient-based optimization. The log-sigmoid activation function is employed because it effectively captures nonlinear input–output relationships while constraining the neuron outputs to the interval $(0, 1)$, thereby facilitating stable learning and improving the interpretability of the network behavior. The log-sigmoid function shows that as inputs grow, outputs grow proportionally when the input values are in the linear part of the function. ANNs are a modern approach to computing, which mimics the human brain structure. These systems are designed to replicate the brain's adaptive processes by executing tasks such as learning, classification, clustering, and prediction with comparable effectiveness. The main benefits of employing the ANN technique are as follows:

- ANNs are incredibly effective and efficient, even when hardware resources are limited.
- The training dataset's results are mostly determined by the input vector.
- The complex mapping of physical elements to response variables is greatly simplified by ANN modeling.
- The weights in the training model are iteratively adjusted to minimize error and enhance prediction accuracy.

Advancements in training methods and interneuronal connectivity have produced diverse neural network architectures. Stratification results from complex connections among neurons. An ANN typically includes input, hidden, and output layers. The ANN processes data sequentially through these layers to generate results. Data moves from the input to the hidden layer via weighted connections. Storing input values and weights in a database supports ANN training. Designing an ANN requires careful consideration of factors, such as the number of layers and the configuration of hidden neurons.

This study presents a hybrid fractional coinfection model for HIV/HBV and a computational framework that integrates ANNs with the LMA to optimize the modeling of HIV/HBV coinfection dynamics. This combined approach effectively addresses highly nonlinear and complex systems that are often intractable using traditional numerical methods. Methodology gives us an accurate approximation of interactions between HIV and HBV, which allows us to develop new approaches for treating the disease. From the results, we can see that the ANN–LMA methodology provides good predictive accuracy and is flexible enough when different parameters are involved. This methodology can be used as an instrument for studying transmission dynamics and control strategies for coinfection of HIV and HBV. Training is fast and does not involve heavy computation. With the help of the Levenberg-Marquardt algorithm, we achieve reliable convergence and steady movement towards the solution. In this study, the sigmoid function is used to train the ANN-LMA algorithm.

The proposed ANN-LMA model is evaluated using three statistical metrics: MSE, RMSE, and regression coefficient (R). Minimizing metric errors is essential for achieving optimal performance, improving operational efficiency, and supporting informed decision-making within industrial applications. Furthermore, low error rates are critical to developing accurate predictive models in artificial intelligence and machine learning. These metrics measure accuracy, error magnitude, and the

correlation between actual and predicted values. The mathematical expressions are defined as follows:

$$\text{MSE} = \frac{1}{n}\sum_{q=1}^{n}(y_q - x_q)^2, \tag{8.5}$$

$$\text{RMSE} = \sqrt{\frac{1}{n}\sum_{q=1}^{n}(y_q - x_q)^2}, \tag{8.6}$$

$$R = \frac{\sum_{q=1}^{n}(x_q - \bar{x})(y_q - \bar{y})}{\sqrt{\sum_{q=1}^{n}(x_q - \bar{x})^2}\sqrt{\sum_{q=1}^{n}(y_q - \bar{y})^2}}, \tag{8.7}$$

where $y_q$ represents the ANN-predicted values, $x_q$ denotes the reference solution values, and $\bar{x}$ and $\bar{y}$ denote the mean values of the exact and predicted data, respectively. $n$ is the total number of data points. These metrics evaluate model performance by measuring error reduction and predictive accuracy against observed data.

Table 3 summarizes the convergence characteristics of the ANN–LMA framework across all model compartments. The network achieved convergence and optimal validation performance for each group in the coinfection HIV/HBV model, as shown in Table 3. All statistical measures confirm the reliability, accuracy, and predictive capability of the proposed ANN-LMA approach. The parameter "Mu" serves as a damping coefficient that regulates the LM optimization process. This coefficient helps the algorithm switch from gradient descent to the Gauss-Newton method when training weights and biases. Table 3 shows the minimum values of MSE and RMSE, which provide further confirmation of the predicted accuracy and validity of the ANN-LMA approach for the coinfection HIV/HBV model. The HIV/HBV coinfection model is numerically simulated using Caputo fractional derivatives for various fractional orders $\alpha = 0.7, 0.75, 0.8, 0.85, 0.9, 0.95$, and 1 to study the memory effect. In the simulation, the initial conditions are selected so that their sum equals 569,000. Initial conditions are taken as follows:

$$\begin{aligned} S(0) = 400000, \quad V(0) = 166900, \quad E_1(0) = 400, \quad E_2(0) = 300, \\ E_3(0) = 350, \quad A_1(0) = 250, \quad A_2(0) = 250, \quad A_3(0) = 250, \\ I_1(0) = 100, \quad I_2(0) = 100, \quad I_3(0) = 50, \quad R(0) = 50. \end{aligned} \tag{8.8}$$

The results indicate that the developed ANN-LMA scheme efficiently captures the behavior of the HIV/HBV coinfection model. The proposed ANN-LMA scheme provides efficient, effective, and reliable results. The simulations are performed within a fixed time interval, where the data set is split into 70% for training, 15% for validation, and 15% for testing phases. A neural network with 20 neurons in the hidden layer is used to approximate the system dynamics. A neural network with 20 neurons in the hidden layer is used to approximate the dynamics of the model under consideration. Most of the data is used for training, and the remainder is used for validation and testing to improve the model's robustness and reliability. Curve fitting is performed using the least squares approach in MATLAB R2024a. Figure 4 shows the fitted model curve to the data, and Table 2 shows the values of the parameters used in the modeling procedure. Figure 5 shows the architecture of the ANN-LMA methodology, which contains two hidden layers with twenty neurons each and an output

layer used in the proposed model. The state of training in neural networks indicates the stability and convergence of the network during training. In this case, the mu parameter is regulated to enhance convergence and avoid overfitting. The gradient is used to measure learning performance; smaller gradient values indicate better learning accuracy in coinfection dynamics. Figure 6 shows training-state plots demonstrating the convergence of the proposed ANN-LMA algorithm in the HIV/HBV coinfection system. In the graph shown, there are gradient values, Mu, and validation checks. A decrease in the value of the Mu parameter in the LMA means stable and fast convergence. Validation checks still equal zero, meaning the validation performance is improving without any early stopping.

**(a)** Training State of $S(t)$ **(b)** Training State of $V_b(t)$ **(c)** Training State of $E_b(t)$

**(d)** Training State of $E_h(t)$ **(e)** Training State of $E_{hb}(t)$ **(f)** Training State of $A_b(t)$

**(g)** Training State of $A_h(t)$ **(h)** Training State of $A_{hb}(t)$ **(i)** Training State of $I_b(t)$

**(j)** Training State of $I_h(t)$ **(k)** Training State of $I_{hb}(t)$ **(l)** Training State of $R_b(t)$

**Figure 6.** Training-state of ANN-LMA scheme for the coinfection model.

Figure 6 presents declining Mu and gradient values over time. Training and testing of the optimum network, along with the optimum convergence of results, are linked to small gradient and Mu values.

The MSE is an extensively utilized statistical measure for analyzing model performance. In the present work, MSE acts as the key measure for determining the efficiency of the suggested algorithm. This measure offers a good yardstick, with gradient values tending towards zero being the best. Small values of MSE are an indicator of good optimization performance. MSE converges quickly at the early stages of training and then becomes stable, demonstrating the successful learning of the network of the system dynamics. Figure 7 demonstrates that the HIV/HBV coinfection model achieved optimal validation performance in each compartment, with values of $1.38E{-}9$, $2.64E{-}11$, $1.31E{-}7$, $2.95E{-}10$, $2.42E{-}9$, $7.04E{-}8$, $1.4E{-}9$, $1.11E{-}10$, $1.25E{-}6$, $8.33E{-}12$, $1.36E{-}8$, and $1.43E{-}9$ recorded across successive epochs. These lowest values indicate the highest level of prediction accuracy achieved by the ANN-LMA scheme. The overlap among the testing, validation, and training curves indicates that the network generalizes effectively and does not exhibit overfitting.

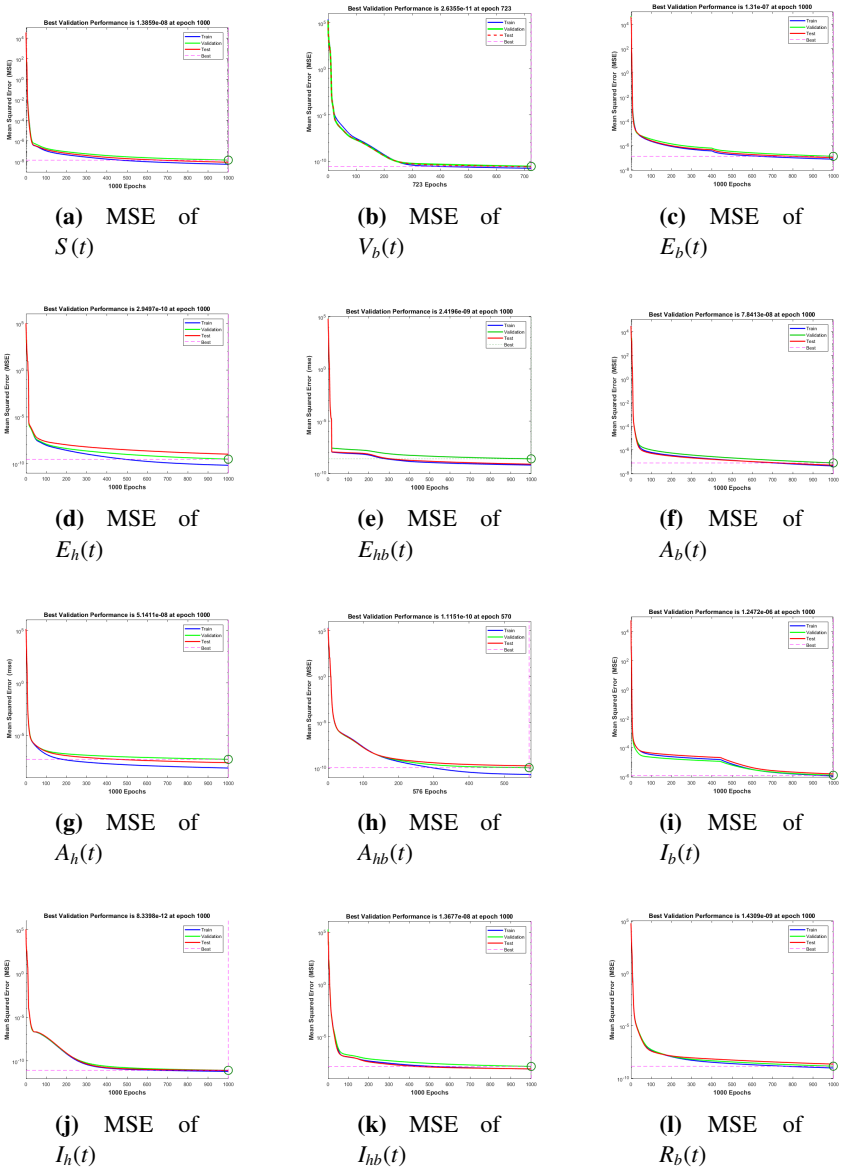

**(a)** MSE of $S(t)$ **(b)** MSE of $V_b(t)$ **(c)** MSE of $E_b(t)$

**(d)** MSE of $E_h(t)$ **(e)** MSE of $E_{hb}(t)$ **(f)** MSE of $A_b(t)$

**(g)** MSE of $A_h(t)$ **(h)** MSE of $A_{hb}(t)$ **(i)** MSE of $I_b(t)$

**(j)** MSE of $I_h(t)$ **(k)** MSE of $I_{hb}(t)$ **(l)** MSE of $R_b(t)$

**Figure 7.** MSE convergence of ANN-LMA scheme for the coinfection model.

Figure 8 presents the time series response plots obtained from the gradient-based performance analysis of the ANNs-LMA model. The graphs demonstrate a uniform distribution of outputs on both sides of the response curve, with minimal errors detected in the training, testing, and validation subgroups. It is clear that the model works well with the data, and there are a few errors in it. This pattern gives us a complete insight about the performance of the ANN-LMA technique. They demonstrate how changing the value of different model parameters affects performance and efficiency. In addition, these graphs keep track of progress during the training process and ensure convergence at each epoch. These graphs represent the dynamics of time and provide information to future studies on how to improve the model through visualization of its reaction over time.

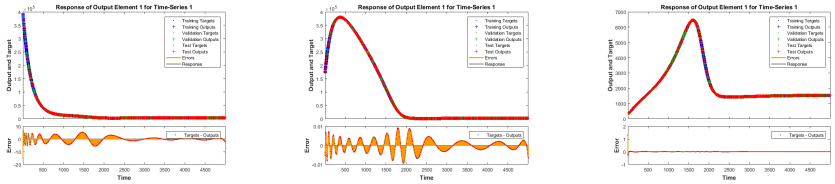

**(a)** Fitness of $S(t)$



**(b)** Fitness of $V_b(t)$



**(c)** Fitness of $E_b(t)$

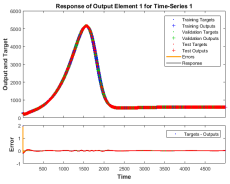

**(d)** Fitness of $E_h(t)$

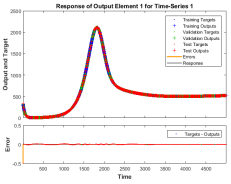

**(e)** Fitness of $E_{hb}(t)$

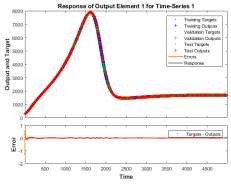

**(f)** Fitness of $A_b(t)$

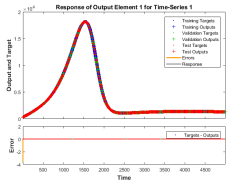

**(g)** Fitness of $A_h(t)$

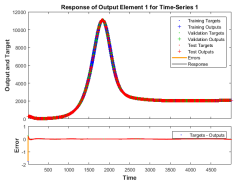

**(h)** Fitness of $A_{hb}(t)$

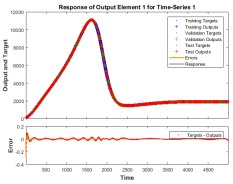

**(i)** Fitness of $I_b(t)$

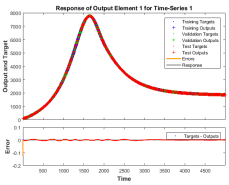

**(j)** Fitness of $I_h(t)$

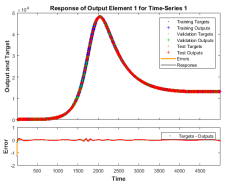

**(k)** Fitness of $I_{hb}(t)$

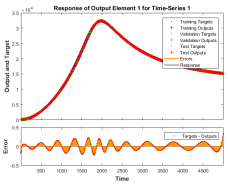

**(l)** Fitness of $R_b(t)$

**Figure 8.** Fitness evaluation of ANN-LMA scheme for the coinfection model.

Figure 9 presents the error histogram with 20 bins for the proposed coinfection HIV/HBV model, illustrating the distribution of prediction errors. Errors in the training, validation, and test sets display

similar patterns and remain close to zero. These results indicate that the neural network accurately and objectively predicts the fractional-order system. Error histograms depend on bias identification, network assessments, and error metrics. Providing timely inputs to the supervised neural network is beneficial. They are effective tools for evaluating neural network capacity and improving foundational performance. Figure 9 presents the error histogram for the HIV/HBV coinfection model, with values of approximately $-1.2E-05$, $6.12E-07$, $1.06E-06$, $-1.06E-06$, $4.443E-06$, $2.52E-06$, $7.49E-05$, $1.23E-06$, $-0.00031$, $4.93E-07$, $-1.8E-05$, and $8.27E-06$. The minimal errors demonstrate that the actual results closely match the expected outcomes.

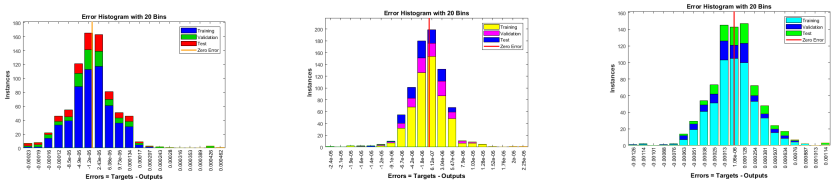

**(a)** Error histogram of $S(t)$



**(b)** Error histogram of $V_b(t)$



**(c)** Error histogram of $E_b(t)$

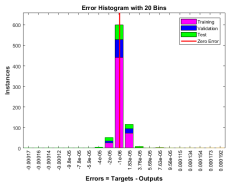

**(d)** Error histogram of $E_h(t)$

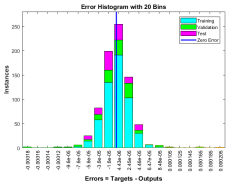

**(e)** Error histogram of $E_{hb}(t)$

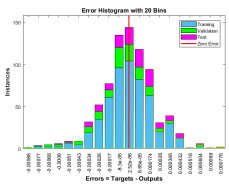

**(f)** Error histogram of $A_b(t)$

**(g)** Error histogram of $A_h(t)$

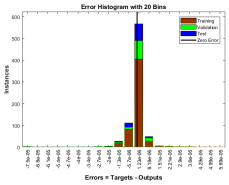

**(h)** Error histogram of $A_{hb}(t)$

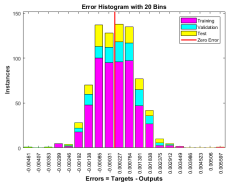

**(i)** Error histogram of $I_b(t)$

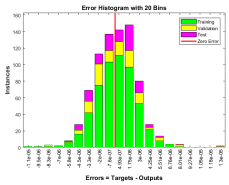

**(j)** Error histogram of $I_h(t)$

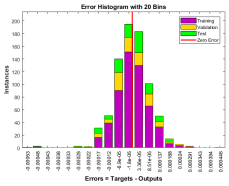

**(k)** Error histogram of $I_{hb}(t)$

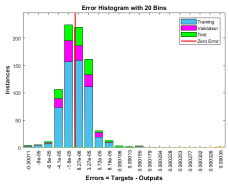

**(l)** Error histogram of $R_b(t)$

**Figure 9.** Error histogram based evaluation of ANN-LMA scheme for the coinfection model.

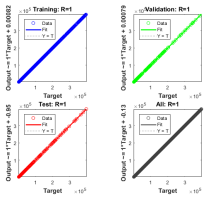

**(a)** Regression analysis of $S(t)$

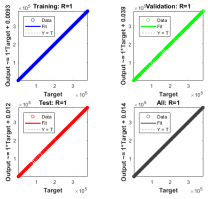

**(b)** Regression analysis of $V_b(t)$

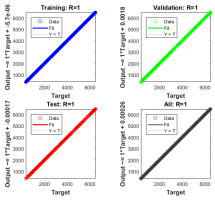

**(c)** Regression analysis of $E_b(t)$

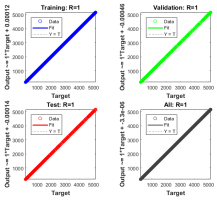

**(d)** Regression analysis of $E_h(t)$

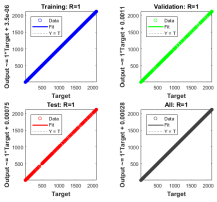

**(e)** Regression analysis of $E_{hb}(t)$

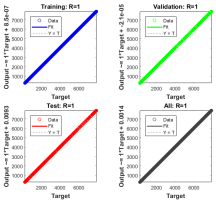

**(f)** Regression analysis of $A_b(t)$

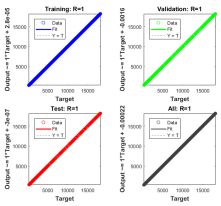

**(g)** Regression analysis of $A_h(t)$

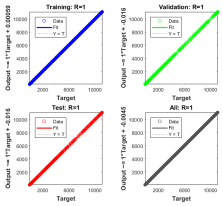

**(h)** Regression analysis of $A_{hb}(t)$

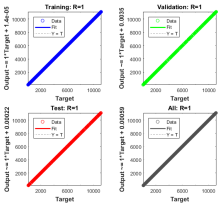

**(i)** Regression analysis of $I_b(t)$

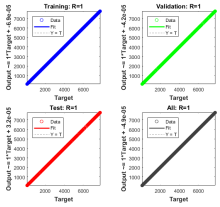

**(j)** Regression analysis of $I_h(t)$

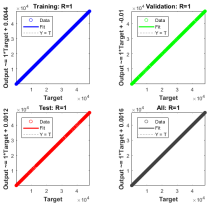

**(k)** Regression analysis of $I_{hb}(t)$

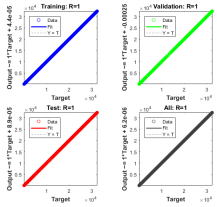

**(l)** Regression analysis of $R_b(t)$

**Figure 10.** Regression analysis of ANN-LMA scheme for the coinfection model.

Regression analysis measures how closely the data gradient matches the model. Curve fitting is optimal when data points align with the linear target line. A higher R-squared value indicates that the data points closely align with the regression line, demonstrating a strong correspondence between the model's predictions and the observed data. A coefficient of variation of 1 indicates that the variability in the dependent variable is attributable to the independent variable in the model, signifying optimal curve fitting. An R value approaching zero indicates the absence of a linear correlation between outputs and targets, whereas an R value of 1 denotes a perfect linear correlation between these variables.

The regression plot illustrates a strong correlation across the dataset, forecasting, solution verification, training procedures, and testing effectiveness, as shown in Figure 10. Regression analysis shows strong alignment between neural network predictions and target values, confirming the proposed model's predictive performance. Figure 10 presents an extensive evaluation of the regression analysis for the proposed model. Since the regression coefficient is equal to $R = 0.9999$, there is an almost perfect correlation between the real and predicted values. The points on the graph fit well into the straight line $Y = T$. This means that the developed algorithm is highly accurate and reliable.

Figure 11 presents the behavior of the model classes as the fractional order ($\alpha$) varies. The impact of $\alpha$ on each compartment is evaluated for the following values: $\alpha = 0.7, 0.75, 0.8, 0.85, 0.90, 0.95$, as well as for the conventional case where $\alpha = 1$. The results demonstrate a reduction in the susceptible population over time, as illustrated in Figure 11(a). The susceptible population declines rapidly from an initial value of $4.0\times10^5$ to below $0.8\times10^5$ within the first 10 time units, then gradually approaches zero by $t \approx 25$, as shown in Figure11(a). Smaller fractional orders accelerate the depletion of susceptibles, whereas the classical case $\alpha = 1$ exhibits a slightly slower decline. An increase in the value of $\alpha$ results in a further reduction of the susceptible population.

Figure 11(b) illustrates the influence of $\alpha$ on the vaccination compartment for HBV. When $\alpha = 0.70$, a smaller peak appears at the initial time, whereas a higher peak is evident at the beginning for $\alpha = 0.95$. At the end of the time period, the decrease for $\alpha = 0.95$ is more significant than for $\alpha = 0.70$. Figure 11(b) shows how $\alpha$ affects the exposed class for HBV. Higher $\alpha$ values produce a smaller initial peak and lower end values over time, while lower $\alpha$ values show the opposite trend. The compartments $E_h$, $E_{hb}$, $A_b$, $A_{hb}$, $I_b$, $I_h$, $I_{hb}$, and $R_b$ in Figure 11(d) to Figure 11(i) exhibit similar behavior. However, Figure 11(g) for $A_h$ displays a distinct pattern, characterized by a pronounced initial peak, rapid decline, and lower final values as $\alpha$ increases. For smaller values of $\alpha$, the peak is significantly higher than for larger values. The curve does not show a sudden drop, and the final values in the time domain remain higher for smaller $\alpha$. Figure 11 presents the numerical dynamics for various fractional orders $\alpha = 0.70$, 0.75, 0.8, 0.85, 0.90, 0.95, and 1.0, as well as the corresponding ANN–LMA approximation solutions. The accuracy of the ANNs-LMA scheme is demonstrated by the overlap of outcomes across compartments in the HIV/HBV coinfection model. Absolute error is a key concept in mathematics and data analysis that quantifies the difference between a measured or calculated value and its true value. It provides valuable insights into the accuracy and reliability of calculations, estimates, and predictive models. In scientific experiments, computational simulations, and statistical analyses, minimizing absolute error is essential for ensuring reliability. Low absolute error indicates that assessments or predictions closely correspond to actual conditions or theoretical expectations, thereby increasing the validity and dependability of the results. ANNs that minimize absolute error deliver better performance in data classification, parameter estimation, and outcome prediction, thereby enhancing their relevance in real-world applications. Analysis of absolute error in ANNs-LMA supports the security and effectiveness of the proposed solution.

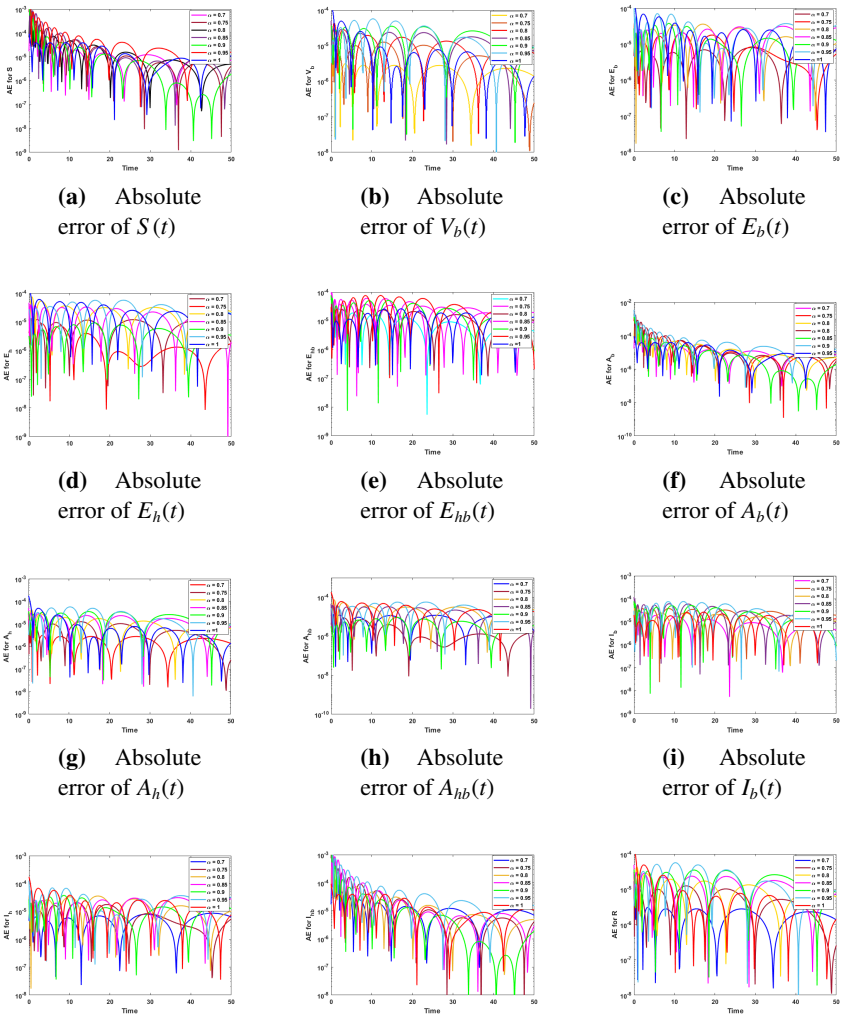

**(a)** Absolute error of $S(t)$ **(b)** Absolute error of $V_b(t)$ **(c)** Absolute error of $E_b(t)$

**(d)** Absolute error of $E_h(t)$ **(e)** Absolute error of $E_{hb}(t)$ **(f)** Absolute error of $A_b(t)$

**(g)** Absolute error of $A_h(t)$ **(h)** Absolute error of $A_{hb}(t)$ **(i)** Absolute error of $I_b(t)$

**(j)** Absolute error of $I_h(t)$ **(k)** Absolute error of $I_{hb}(t)$ **(l)** Absolute error of $R_b(t)$

**Figure 11.** Minimal absolute errors using ANN-LMA approach for HIV/HBV coinfection dynamics.

Figure 12 shows the absolute error for each compartment in the fractional-order coinfection model. The absolute error for each compartment ranges approximately from $E-03$ to $E-09$, $E-04$ to $E-09$, $E-04$ to $E-09$, $E-04$ to $E-09$, $E-04$ to $E-09$, $E-03$ to $E-10$, $E-04$ to $E-09$, $E-04$ to $E-09$, $E-04$ to $E-09$, $E-04$ to $E-08$, $E-03$ to $E-08$, and $E-04$ to $E-09$, respectively. The findings suggest that the proposed ANNs-LMA technique achieves higher accuracy and efficiency.

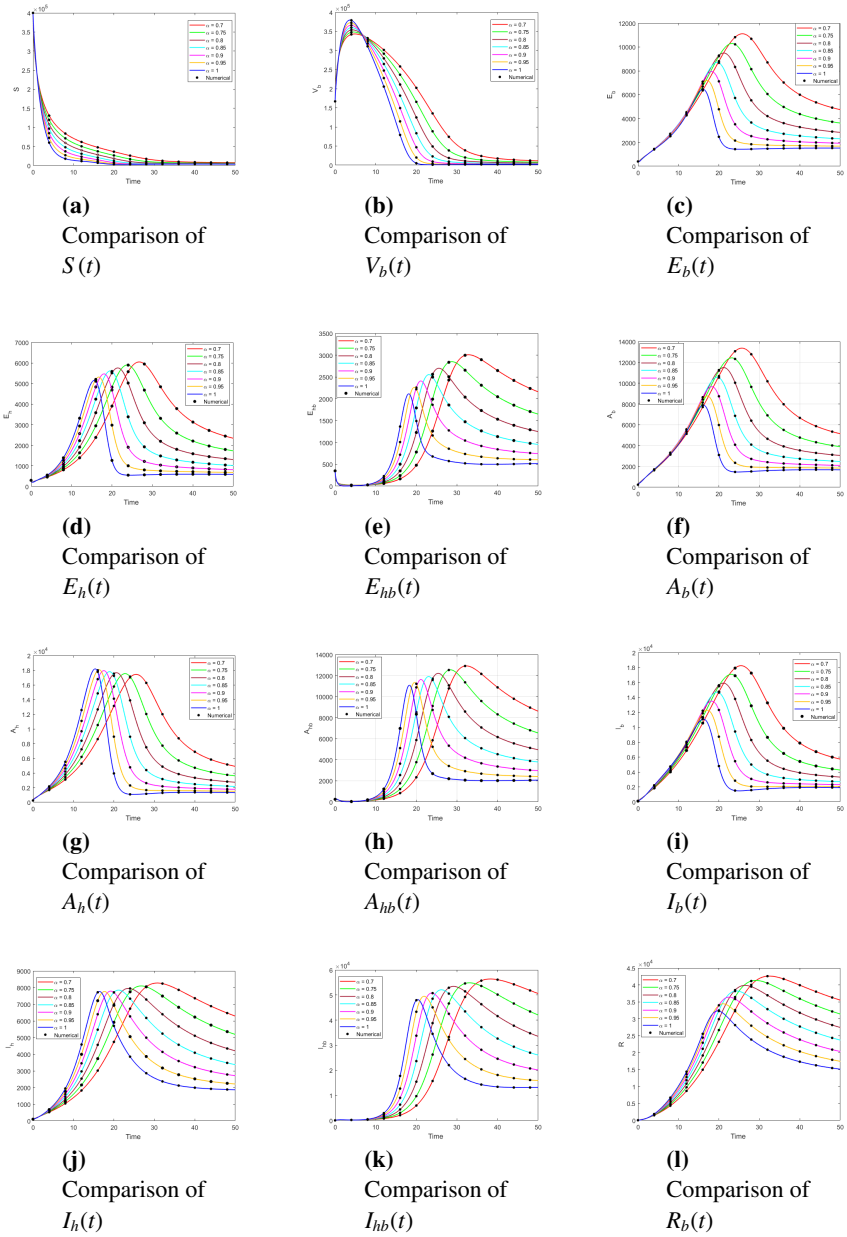

**(a)** Comparison of $S(t)$

**(b)** Comparison of $V_b(t)$

**(c)** Comparison of $E_b(t)$

**(d)** Comparison of $E_h(t)$

**(e)** Comparison of $E_{hb}(t)$

**(f)** Comparison of $A_b(t)$

**(g)** Comparison of $A_h(t)$

**(h)** Comparison of $A_{hb}(t)$

**(i)** Comparison of $I_b(t)$

**(j)** Comparison of $I_h(t)$

**(k)** Comparison of $I_{hb}(t)$

**(l)** Comparison of $R_b(t)$

**Figure 12.** Comparative analysis of HIV/HBV coinfection model.

Combining the numerical modeling approach with estimated data enables accurate simulation-based forecasting and assessment of epidemic dynamics. The computational techniques provide important information about epidemics, their prevention, and control, thus connecting the theoretical framework with practice in healthcare. They are vital in making scientific discoveries, informing health policy decisions, and enhancing global health. The effectiveness of ANNs-LMA is validated by key performance indicators, which demonstrate good accuracy in evaluating the proposed HIV/HBV co-infection model. The results show that the ANNs-LMA approach yields more accurate, efficient, and reliable predictions. The application of the ANNs-LMA scheme shows superior performance compared to traditional techniques. The ANNs-LMA demonstrate strong reliability, as evidenced by

consistent performance metrics and low error rates. As can be seen, the low absolute error values indicate that the method has good accuracy and reliability, making it suitable for computational use. It is clear from the above discussion that the ANN-LMA approach is applicable to solving practical problems using computation. This allows researchers to improve the evaluation of disease trends using the ANN, making it more applicable in the medical field. The performance measures serve as criteria for optimizing the ANN's performance. Based on the above outcomes, we thoroughly assess the results to confirm the framework's strengths, effectiveness, and reliability, as well as the performance improvements achieved. Evaluations show the model is highly accurate and resilient with complex data. The absolute error is significantly reduced, validating the model's efficacy for complex applications. These results support further research and reinforce confidence in ANN's for advanced prognostic forecasting.

### *8.1. Limitations and future work*

The suggested model of coinfection is a good fit, but an unrealistic representation of the spread of HIV/HBV. This is because the behavior of the two diseases' epidemics is heavily influenced by risky behavior among specific subgroups of the infected population. One of the model's limitations suggests directions for future research. Specifically, the model assumes homogeneous mixing within each compartment, which precludes the incorporation of additional dynamics that may influence the transmission of viral coinfection, such as HIV/HBV. The limited number of samples for parameter estimation poses a limitation. Nevertheless, sensitivity analysis and the estimation period can help validate the model's robustness to some extent. The designed ANN-LMA methodology achieves high accuracy in estimating the numerical solution of the investigated fractional-order epidemiological model. Apart from approximation of solutions, the ANN can forecast epidemic dynamics provided that the system's dynamics exhibit characteristics similar to those learned by the trained neural network. The present analysis uses data from a fractional coinfection HIV/HBV model, in which the fixed parameters and initial conditions were based on the real dataset. The model's generalization capability remains limited when applied to epidemiological cases with varying transmission rates, initial case numbers, intervention strategies, or dynamic intervention controls. To improve the applicability of the proposed ANN framework in epidemiology, future research should focus on training the model with data from diverse parameter settings and intervention scenarios.

The model demonstrates strong performance in viral coinfection modeling by capturing the dynamics between two pathogens across different stages of disease progression. The developed framework and neural network approach are adaptable to infection data from various regions, especially in populations affected by HIV/HBV coinfections. Implementing this modification is expected to improve the model's robustness and allow the network to capture a wider range of disease transmission patterns. Although the current ANN-LMA methodology provides an accurate and efficient computational solution, its predictive use in novel outbreak scenarios requires caution until further generalization studies are completed. In the future, the proposed fractional and AI-based neural network methods could be applied across a range of fields [42–46].

## 9. Conclusions

This research introduces a novel fractional-order mathematical model that analyzes the co-dynamics of HIV/HBV coinfection using an ANNs-LMA scheme. This study evaluates the effectiveness of an ANNs-LMA scheme for analyzing the transmission dynamics of HIV/HBV coinfection across various transmission routes. It further examines the potential impact of vaccination on these dynamics and the progression of both HIV and HBV in affected individuals. Another important aspect of this modeling is analyzing the performance of the ANN-LMA across different values of the Caputo fractional order. The primary contributions and objectives of this study are as follows:

- A novel co-infection HIV/HBV model is developed, and the ANN-LMA scheme is employed to accurately capture the dynamics of the proposed system. The solutions of the HIV/HBV co-infection model have been effectively demonstrated using an ANN-LMA scheme.
- To minimize MSE, the dataset was split into three parts: 70% for training, 15% for testing, and 15% for validation. During the training stage of the proposed scheme, the MSE approaches zero, indicating that the proposed solutions approximate the target with high precision. This minimal error demonstrates the model's high accuracy and exceptional results.
- The optimization was executed with LMA.
- The accuracy of the proposed developed ANN-LMA has been evidenced by the overlapping results and lower MSE.
- The absolute error values are approximately computed between $10^{-3}$ to $10^{-9}$, which results in validating the accuracy of the technique.
- Additional metrics, including regression analysis, training state, and error histograms evaluations, confirm the accuracy of the proposed ANN-LMA scheme.

Currently, there is a lack of models addressing coinfection HIV/HBV transmission patterns within the population. To address this gap, a compartmental fractional order mathematical model was developed. The significance of this hybrid study lies in its use of a mathematical model that integrates neural networks into health care systems, highlighting the role of AI-based models in understanding disease transmission. The ANN-LMA offers an excellent platform for understanding the nature of coinfection and its prediction. ANN-LMA can be used as an efficient model for studying coinfection dynamics, testing different scenarios, and making predictions using real-world data.

## Author contributions

Muhammad Asad Ullah: Writing-original draft, Software, Formal analysis, Data curation; Sana Ullah Saqib: writing-original draft, software, formal analysis, data curation, review & editing, methodology, visualization; Yin-Tzer Shih: Conceptualization, Writing-review & editing, Supervision; Nermeen Abdullah: Writing-original draft, Software, Investigation, Review & editing, Methodology, Visualization, Supervision; Nidhal Becheikh: Conceptualization, Writing-review & editing; Lioua Kolsi: Writing-review & editing, Visualization, Methodology. Kaouther Ghachem: Software, Formal analysis, Data curation, Review & editing, Methodology. All authors have read and approved the final version of the manuscript for publication.

## Use of Generative-AI tools declaration

The authors declare that no generative Artificial Intelligence (AI) tools were used in the writing or development of this article.

## Acknowledgments

The authors would like to thank the anonymous referees for their kind comments and valuable suggestions. The second and third authors gratefully acknowledge the support of the National Science and Technology Council (NSTC), Taiwan, through the NSTC project under Grant No. NSTC 114-2115-M-005-002-MY2. Princess Nourah bint Abdulrahman University Researchers Supporting Project number (PNURSP2026R730), Princess Nourah bint Abdulrahman University, Riyadh, Saudi Arabia. The authors extend their appreciation to the Deanship of Scientific Research at Northern Border University, Arar, KSA, for funding this research work through the project number "NBU-FPEJ-2026-2933-04".

## Conflict of interest

The authors declare there are no conflist of interest.

## References

1. A. Kaur, G. S. Randhawa, A. A. Farooque, M. Ali, H. Singh, K. Al-Mughrabi, et al., Crop disease surveillance through integration of machine and deep learning in the face of climate change, *Journal of Agriculture and Food Research*, **26** (2026), 102733. http://doi.org/10.1016/j.jafr.2026.102733
2. Q. L. Wu, L. Zhi, M. H. Yao, B. Bai, C. Wang, Y. Niu, Vibrations analysis and neural network prediction of the locust-leg-inspired tubes, *Nonlinear Dyn.*, **114** (2026), 390. http://doi.org/10.1007/s11071-025-12132-w
3. S. K. Sinha, S. Prabha, N. K. Goyal, N. Srivastava, Deep learning techniques for the prediction of heart disease, In: *Intelligent systems using semiconductors for robotics and IoT*, New York: CRC Press, 2025, 371–374.
4. K. Guedri, R. Zarin, M. Oreijah, S. K. Alharbi, H. A. El-Wahed Khalifa, Artificial neural network-driven modeling of Ebola transmission dynamics with delays and disability outcomes, *Comput. Biol. Chem.*, **115** (2025), 108350. http://doi.org/10.1016/j.compbiolchem.2025.108350
5. S. Chae, S. Kwon, D. Lee, Predicting infectious disease using deep learning and big data, *Int. J. Environ. Res. Public Health*, **15** (2018), 1596. http://doi.org/10.3390/ijerph15081596
6. A. Di Bella, M. Raissi, D. Santoro, P. Roccaro, Physics-informed neural networks in water and wastewater systems: A critical review, *Water Res.*, **293** (2026), 125449. http://doi.org/10.1016/j.watres.2026.125449

7. W. H. Fan, X. J. Chen, Embedding physics into machine learning: A review of physics informed neural networks as partial differential equation forward solvers, *Tsinghua Sci. Technol.*, **31** (2026), 1326–1364. http://doi.org/10.26599/TST.2025.9010157
8. G. Aruta, F. Ascione, N. Bianco, G. M. Mauro, F. Villano, Artificial neural networks to forecast building heating/cooling demand and climate resilience based on envelope parameters and new climatic stress indices, *J. Build. Eng.*, **108** (2025), 112849. http://doi.org/10.1016/j.jobe.2025.112849
9. L. Alnaji, Machine learning in epidemiology: neural networks forecasting of Monkeypox cases, *PLoS One*, **19** (2024), e0300216. http://doi.org/10.1371/journal.pone.0300216
10. Y. Qian, K. Zhang, E. Marty, A. Basu, E. B. O'dea, X. Q. Wang, et al., Physics-informed deep learning for infectious disease forecasting, *J. R. Soc. Interface.*, **22** (2025), 20250379. http://doi.org/10.1098/rsif.2025.0379
11. M. Rama, G. Santin, G. Cencetti, M. Tizzoni, B. Lepri, Forecasting seasonal influenza epidemics with physics-informed neural networks, *Epidemics*, **55** (2026), 100919. http://doi.org/10.1016/j.epidem.2026.100919
12. P. Guo, T. Liu, Q. Zhang, L. Wang, J. P. Xiao, Q. Y. Zhang, et al., Developing a dengue forecast model using machine learning: A case study in China, *PLoS Negl. Trop. Dis.*, **11** (2017), e0005973. http://doi.org/10.1371/journal.pntd.0005973
13. M. Raissi, P. Perdikaris, G. E. Karniadakis, Physics-informed neural networks: A deep learning framework for solving forward and inverse problems involving nonlinear partial differential equations, *J. Comput. Phys.*, **378** (2019), 686–707. http://doi.org/10.1016/j.jcp.2018.10.045
14. A. Asghar, M. Umar, S. Salahshour, B. Souayeh, H. Alfannakh, S. S. K. Raju, Meningitis epidemic model analysis using artificial neural networks: A Levenberg-Marquardt backpropagation neural network approach, *J. Eng. Res.*, **14** (2026), 1615–1626. http://doi.org/10.1016/j.jer.2026.01.013
15. A. Din, Neural network assisted stability exploration of a stochastic Hepatitis B model incorporating dual transmission routes routes and immune response, *J. Appl. Math. Comput.*, **72** (2026), 116. http://doi.org/10.1007/s12190-026-02770-7
16. Z. Sabir, T. Botmart, M. A. Z. Raja, W. Weera, R. Sadat, M. R. Ali, et al., Artificial neural network scheme to solve the nonlinear influenza disease model, *Biomed. Signal Proces.*, **75** (2022), 103594. http://doi.org/10.1016/j.bspc.2022.103594
17. P. A. Naik, B. M. Yeolekar, S. Qureshi, M. Yeolekar, A. Madzvamuse, Modeling and analysis of the fractional-order epidemic model to investigate mutual influence in HIV/HCV co-infection, *Nonlinear Dyn.*, **112** (2024), 11679–11710. http://doi.org/10.1007/s11071-024-09653-1
18. P. A. Naik, M. O. Kulachi, A. Ahmad, M. Farman, F. Iqbal, M. Taimoor, et al., Modeling different strategies towards control of lung cancer: leveraging early detection and anti-cancer cell measures, *Comput. Method. Biomec.*, **29** (2026), 603–617. http://doi.org/10.1080/10255842.2024.2404540
19. S. U. Saqib, A. Hasan, Y. T. Shih, A novel hybrid fractional approach to nonlinear dynamics of HIV transmission among men who have sex with men in Taiwan, *AIMS Mathematics*, **10** (2025), 13204–13230. http://doi.org/10.3934/math.2025592

20. A. Khan, A. Mukheimer, T. Abdeljawad, R. Thinakaran, Data-driven modeling and simulation of Caputo–Fabrizio fractional order shingles disease model, *AIMS Mathematics*, **11** (2026), 5992–6018. http://doi.org/10.3934/math.2026248

21. V. Muthupandi, A. J. Gnanaprakasam, S. Boulaaras, Fractional order modeling of hepatitis C transmission dynamics with physics-informed neural network solutions, *BMC Infect. Dis.*, **26** (2026), 457. http://doi.org/10.1186/s12879-026-12792-y

22. P. Varshney, G. R. Naunyal, S. Kumar, A high-precision Bernstein wavelet neural network modeling for solving fractional-order brucellosis infection models, *Phys. Scr.*, **101** (2026), 066002. http://doi.org/10.1088/1402-4896/ae3fe1

23. M. Umar, S. Salahshour, N. Akoum, W. Ishaq, U. Baltaeva, Fractional-order modeling of infectious diseases: A stochastic neural network procedure to deal with vaccination and awareness strategies, *Netw. Model. Anal. Health Inform. Bioinforma.*, **15** (2026), 49. http://doi.org/10.1007/s13721-026-00734-2

24. M. A. Stephano, J. N. Mlyahilu, I. H. Jung, Modelling lymphatic filariasis dynamics using Levenberg–Marquardt algorithm-artificial neural networks, *Results in Control and Optimization*, **22** (2026), 100659. http://doi.org/10.1016/j.rico.2026.100659

25. Eiman, K. Shah, M. Sarwar, T. Abdeljawad, Study of fractional order epidemic compartmental model by using artificial deep neural networks, *Neural Networks*, **192** (2025), 107944. http://doi.org/10.1016/j.neunet.2025.107944

26. K. S. Nisar, M. Farman, M. Waseem, M. A. Ahmed, M. Hafez, Computational framework and machine learning approach to fractional order soil helminth infections disease model for control mechanism, *Sci. Rep.*, **16** (2026), 6671. http://doi.org/10.1038/s41598-026-36701-0

27. I. Ahmed, M. Amjid, E. Azhar, M. Jamal, Z. Faiz, Fractional order modeling and solution of West Nile virus epidemic model in presence of Wolbachia, *Comput. Biol. Med.*, **196** (2025), 110652. http://doi.org/10.1016/j.compbiomed.2025.110652

28. T. Liu, B. L. Ding, A radial basis function neural network approach for solving a diffusion partial differential equation efficiently, *Appl. Math. Comput.*, **509** (2026), 129651. http://doi.org/10.1016/j.amc.2025.129651

29. I. H. Lee, S. Saqib, Q. Sheng, Y.-T. Shih, An epidemiological model of the mumps virus via Mittag-Leffler Kernel: Stability analysis and artificial neural network solutions, *AIMS Mathematics*, **10** (2025), 24923–24957. http://doi.org/10.3934/math.20251103

30. M. W. Anjum, S. U. Saqib, Y.-T. Shih, I. H. Jaghdam, N. Becheikh, L. Kolsi, An intelligent soft computing model for predicting the thermal behavior of blood-based trihybrid nanofluids flow in biomedical drug delivery applications, *Case Stud. Therm. Eng.*, **74** (2025), 106742. http://doi.org/10.1016/j.csite.2025.106742

31. S. U. Saqib, Y.-T. Shih, M. W. Anjum, M. Shoaib, Advanced heuristic computing with Gudermannian neural networks for mathematical modeling of divorced dynamics in social networks, *Math. Comput. Simulat.*, **239** (2026), 745–765. http://doi.org/10.1016/j.matcom.2025.07.048

32. S. U. Saqib, S.-H. Fang, M. A. Z. Raja, K. S. Nisar, M. Shoaib, Design of intelligent neuro-supervised deep learning networks to analyze brain electrical activity rhythms of Parkinson's disease model, *Cogn. Neurodyn.*, **20** (2026), 32. http://doi.org/10.1007/s11571-025-10404-0
33. M. A. Ullah, N. Raza, A. Omame, M. S. Alqarni, A new co-infection model for HBV and HIV with vaccination and asymptomatic transmission using actual data from Taiwan, *Phys. Scr.*, **99** (2024), 065254. http://doi.org/10.1088/1402-4896/ad4b6c
34. *Centers for Disease Control and Prevention, Hepatitis b–surveillance guidance*, Centers for Disease Control and Prevention. Available from: https://www.cdc.gov/hepatitis/statistics/surveillanceguidance/HepatitisB.htm.
35. P. Van den Driessche, J. Watmough, Reproduction numbers and sub-threshold endemic equilibria for compartmental models of disease transmission, *Math. Biosci.*, **180** (2002), 29–48. http://doi.org/10.1016/S0025-5564(02)00108-6
36. E. X. DeJesus, C. Kaufman, Routh-Hurwitz criterion in the examination of eigenvalues of a system of nonlinear ordinary differential equations, *Phys. Rev. A*, **35** (1987), 5288. http://doi.org/10.1103/PhysRevA.35.5288
37. N. Raza, M. A. Ullah, M. Y. Alshahrani, A. Omame, A. Hayat, Computational aspects and dynamical analysis of a novel HIV/AIDS transmission model with fractional temporal evolution, *Math. Comput. Simulat.*, **240** (2026), 803–822. http://doi.org/10.1016/j.matcom.2025.07.040
38. *Centers for Disease Control, R.O.C. (Taiwan), Home*, 2024, accessed: 2026-02-21. Available from: https://www.cdc.gov.tw/Category/Page/rCV9N1rGUz9wNr8lggsh2Q
39. *Worldometer, Population of countries*, 2026, accessed: 2026-02-21. Available from: https://www.worldometers.info/world-population/population-by-country.
40. *World Population Review, Cities in Taiwan*. Available from: https://worldpopulationreview.com/countries/cities/taiwan.
41. E. E. Endashaw, T. T. Mekonnen, Modeling the effect of vaccination and treatment on the transmission dynamics of hepatitis B virus and HIV/AIDS coinfection, *J. Appl. Math.*, **2022** (2022), 5246762. http://doi.org/10.1155/2022/5246762
42. T. Liu, R. Q. Xue, A convergent multi-step efficient iteration method to solve nonlinear equation systems, *J. Appl. Math. Comput.*, **71** (2025), 2571–2588. http://doi.org/10.1007/s12190-024-02324-9
43. T. Liu, B. L. Ding, F. Soleymani, Risk quantification using Rayleigh-Tail modeling framework: A theoretical study and numerical simulations, *Comput. Appl. Math.*, **45** (2026), 173. http://doi.org/10.1007/s40314-025-03477-4
44. Y. C. Liu, Y. L. Li, T. Liu, An RBF–FD method for pricing under the Bates model: Handling stochastic volatility and jump processes, *Eng. Anal. Bound. Elem.*, **183** (2026), 106622. http://doi.org/10.1016/j.enganabound.2025.106622
45. Y. W. Chen, J. C. Duan, D. H. Li, G. L. Li, Stability and bifurcation in an ecological system under time-dependent environmental influences, *Nonlinear Dyn.*, **113** (2025), 28601–28616. http://doi.org/10.1007/s11071-025-11587-1

46. J. C. Duan, Z. C. Wei, G. L. Li, D. H. Li, C. Grebogi, Strange nonchaotic attractors in a class of quasiperiodically forced piecewise smooth systems, *Nonlinear Dyn.*, **112** (2026), 12565–12577. http://doi.org/10.1007/s11071-024-09678-6


AIMS Press